Cell competition reprograms adherent-suspension plasticity in disseminated tumor cells

Hyunbin D. Huh[1]†, Yujin Sub[2]†, Jee Hung Kim[3,4], Hannah Lee[1], Jongwook Oh[2], Dong Ki Lee[3], Jong Hwa Byun[1], Woo Yang Pyun[1], Sehyung Pak[5], Junjeong Choi[6], Tadayoshi Hashimoto[7], Takayuki Yoshino[7], Joon Jeong[3,4]*, Heon Yung Gee[2]*, and Hyun Woo Park[1]*

[1] Department of Biochemistry, College of Life Science and Biotechnology, Brain Korea 21 Project, Yonsei University; Seoul 03722, Republic of Korea.

[2] Department of Pharmacology, Graduate School of Medical Science, Brain Korea 21 Project, Yonsei University College of Medicine; Seoul 03722, Republic of Korea.

[3] Division of Medical Oncology, Department of Internal Medicine, Gangnam Severance Hospital, Yonsei University College of Medicine, Seoul, Korea.

[4] Institute for Breast Cancer Precision Medicine, Yonsei University College of Medicine, Seoul, Republic of Korea.

[5] Cytogen, Seoul, Republic of Korea

[6] College of Pharmacy, Yonsei Institute of Pharmaceutical Sciences, Yonsei University, Incheon, Republic of Korea.

[7] Department of Gastroenterology and Gastrointestinal Oncology, National Cancer Center Hospital East, Kashiwa, Japan.

† Equal contributions

*Corresponding authors. Email: Hyun Woo Park (hwp003@yonsei.ac.kr), Heon Yung Gee (hygee@yuhs.ac), Joon Jeong (gsjjoon@yuhs.ac)

Abstract

Cell competition within the primary tumor drives tumor growth by promoting the uncontrolled proliferation of winner cells and eliminating loser cells by sensing cell fitness. However, the mechanism of how cell competition confers the loser cells with the metastatic potential of circulating tumor cells (CTCs) to transit between dissemination and colonization remains elusive. Here we found cell competition gives rise to less fit but viable cells that transformed into CTCs via adherent-to-suspension transition (AST) mechanisms. The induction of hematopoietic transcription factors hijacked by solid tumor cells rendered CTCs competent to reprogram their anchorage dependency and disseminate into the bloodstream, while subsequent suppression of these factors was critical to regain adhesion and colonize metastatic lesions. Disrupting the oscillatory dynamics of AST factors blocked the adherent-suspension plasticity (ASP) of breast cancer CTCs and suppressed lung metastasis. Furthermore, multiregional single-cell transcriptomic analyses of matched primary tumors, CTCs, and metastatic lesions from *de novo* metastatic breast cancer patients demonstrate the critical role of ASP in metastasis.

Significance

We demonstrate cell competition-mediated displacement of loser cells manifests dynamic oscillation of AST factors that confer anchorage plasticity to circulating tumor cells critical for their dissemination and colonization in metastasis. These findings highlight the potential of targeting AST factors to develop effective anti-metastatic therapies.

Introduction

Cell competition in multicellular organisms plays a crucial role in maintaining tissue homeostasis by eliminating less-fit cells and allowing competitive cells to thrive. This fitness-driven selection process operates through mechanical competition that depends on cell-cell interactions or molecular competition driven by secreted factors by neighboring cells. In primary tumors, cell competition is increasingly recognized as a driving force of evolution, facilitating clonal expansion of aggressive cells while displacing weaker cells from the tumor niche. Intriguingly, recent evidence suggests that a rare population of displaced, less-fit cells may not simply be passively eliminated but rather actively reprogrammed to contribute to metastasis and recurrence.

Metastasis, the primary cause of cancer death, involves the dissemination of primary tumor cells into the bloodstream as circulating tumor cells (CTCs), their survival within the circulation, and eventual colonization of distant organs. The metastatic cascade, therefore, could be perceived as a consequence of cancer cells constantly transitioning between an adherent state and a suspension state. Based on these observations, we and others recently discovered a biological phenomenon referred to as adherent-to-suspension transition (AST), a mechanism orchestrated by the induction of specific hematopoietic transcription factors, collectively termed AST factors, that reprograms the anchorage dependency of solid tumor cells to facilitate the dissemination and release of CTCs via downregulation of cell-matrix adhesion pathways and induction of anoikis resistance by mitigating oxidative stress. However, whether cell competition during cancer progression confers dynamic plasticity of AST-mediated hematopoietic mimicry to disseminated tumor cells that endows successful completion of the metastatic cascade remains unknown.

66 Here, to investigate the role of adherent-suspension plasticity (ASP) in CTCs during the
67 dissemination and colonization processes, we recapitulated cell competition *in vitro* through
68 dissemination assay, which enabled a rare population of cancer cells to undergo spontaneous
69 detachment and reattachment from a highly confluent and unfavorable cell culture condition that
70 mimics the tumor microenvironment. Surprisingly, these *in vitro* CTC-like cells showed dynamic
71 oscillation of AST factor expression, which emerged during detachment and subsequently
72 suppressed in the course of reattachment. We further show that *in vitro* CTC-like cells reflect
73 similar characteristics to *in vivo* AST-positive CTCs derived from an orthotopic model of breast
74 cancer metastasis.

75 The establishment of advanced patient cohorts that consist of matched primary tumors,
76 CTCs, and metastatic lesions from combined tissue and liquid biopsy specimens provides
77 invaluable insights to reveal undescribed mechanisms, targets, and theories of metastatic plasticity.
78 Thus, moving forward from current multi-omics analyses[1-5], we newly enrolled untreated *de novo*
79 metastatic breast cancer patients, collected matched tissue and liquid biopsy specimens and
80 analyzed single-cell level transcriptomes of paired primary tumors, CTCs, and metastatic lesions.
81 It was necessary to compare the transcriptome of CTCs with their matched solid tumor
82 counterparts harvested from the same patient to monitor the dynamic plasticity of AST factors and
83 related gene signatures within the metastatic cascade from dissemination to colonization. Thus,
84 through the development of a cell competition assay and analyzing single-cell-level transcriptomes
85 of matched specimens from *de novo* metastatic breast cancer patients, our study reveals how
86 anchorage plasticity drives the metastatic cascade via AST factor-mediated ASP in disseminated
87 CTCs.
88

Results

Cell competition reprograms loser cells with AST-mediated anchorage plasticity

Metastasis could be conceived as a longitudinal sequence of cancer cells constantly transitioning between their adherent and suspension states. Solid tumors shed CTCs through a fitness-based cell competition mechanism within the overcrowded environment of the primary tumor. Here, we asked whether the rare population of displaced, less-fit cells are actively reprogrammed to confer metastatic traits of CTCs rather than simply being passively eliminated.

To examine the mechanism underlying the displacement of loser cells from adherent parental cells, we induced cell competition by challenging various subtypes of breast cancer cell lines, including MDA-MB-231, MCF7, BT549, and Hs578T cells, to high cell density stress conditions. Notably, many breast cancer cell lines subjected to overcrowded cell competition exhibited cell-cell contact inhibition or cell death. In MDA-MB-231 cells, however, cell competition induced cell rounding and spontaneous detachment of CTC-like cancer cells that resemble the rare population of disseminated CTCs *in vivo* (**Fig. 1A-B**). We hypothesized that the ability of a cell line to produce CTC-like cells through cell competition would likely reflect its metastatic capacity *in vivo*. To test this, we injected each breast cancer cell line into the fat pad of mice and examined their metastatic efficiency to disseminate and colonize the lung (**Fig. 1C**). As expected, despite showing similar primary tumor growth, the cell lines that failed to generate CTC-like cells via cell competition assay showed significantly lower metastatic potential and prolonged survival compared to MDA-MB-231 (**Fig. 1D**). These observations are in line with earlier reports that classified MDA-MB-231 as one of the most metastatic breast cancer cell lines in mouse models (**Fig. S1A**) [6]. Thus, these results suggest that the metastatic potential of breast cancer cells

112 correlates with the ability to produce spontaneously suspended CTC-like cells via cell competition
113 assay.

114 Next, to identify the molecular characteristics of cell competition-induced CTC-like cells,
115 adherent parental cells and suspended CTC-like cells were subjected to single-cell RNA
116 sequencing analysis (**Fig. 1E**). Interestingly, parental cells and CTC-like cells formed distinct
117 clusters and GSEA analysis revealed that parental cells exhibited significant enrichment in gene
118 sets associated with cell-matrix adhesion, substrate adhesion-dependent cell spreading, and stress
119 fiber assembly compared to CTC-like cells, which indicates active downregulation of anchorage
120 dependence is a hallmark of CTC-like cells (**Fig. 1F-G**). Notably, CTC-like cells exhibited a
121 significant reduction in the expression of genes involved in focal adhesion formation, a process
122 essential for CTCs to detach from the extracellular matrix and disseminate from the primary tumor
123 (**Fig. 1H**). Recent reports have demonstrated the role of YAP1 and TEAD to resist mechanical
124 pressures and confer growth advantage to tumors while the Hippo pathway, a negative regulator
125 of YAP-TEAD, promotes cell-matrix dissociation and detachment of cancer cells from the primary
126 tumors. Interestingly, our results show gene sets associated with Hippo signaling and the
127 expression of core mediators of the Hippo pathway significantly reduced in CTC-like cells
128 compared to parental cells (**Fig. 1I-J**). These results suggest that cell competition renders CTC-
129 like cells competent to undergo spontaneous detachment from the matrix (**Fig. 1K**).

130 We firstly reported that solid tumor cells could spontaneously disseminate CTCs through
131 reprogramming anchorage dependency via the aberrant expression of hematopoietic transcription
132 factors referred to as adherent-to-suspension transition (AST) factors, IKZF1, IRF8, NFE2, and
133 BTG2, which evoke global suppression of integrin-ECM expression, inhibition of YAP-TEAD
134 activity, and induction of hemoglobin that resists anoikis. Thus, we sought to investigate whether

135 cell competition reprograms loser cells with AST-related mechanisms. Surprisingly, cell
136 competition-induced CTC-like cells recapitulated the aberrant induction of endogenous AST
137 factors in MDA-MB-231, which recapitulate are previous findings in CTCs derived from mouse
138 models and *de novo* metastatic breast cancer patients (**Fig. 1L**). scRNA-seq and qPCR results both
139 indicate the significant expression of AST factors in CTC-like cells, but not in their adhesive
140 counterparts (**Fig. 1M-P**). It is important to note that, in contrast to cell competition-induced CTC-
141 like cells, trypsinization-induced passive detachment of cells fails to evoke the expression of AST
142 factors (**Fig. S1B**). To verify whether the induction of AST factors is a prerequisite for the
143 spontaneous detachment of CTC-like cells, we depleted each factor by siRNA and measured the
144 viability of detached cells produced during cell competition. While combinatorial induction of four
145 factors enhances the reprogramming efficiency, we found depletion of any single AST factor was
146 sufficient to markedly suppress the formation of CTC-like cells (**Fig. 1Q**). Moreover, we found
147 that pretreatment with thalidomide-derivatives such as lenalidomide or pomalidomide, which we
148 previously identified as potential anti-metastatic agents that act by reducing the expression of
149 IKZF1 in mouse breast cancer models [7], substantially suppressed the formation of CTC-like cells
150 (**Fig. 1R**). These results demonstrate that cell competition reprograms anchorage dependency of
151 adherent tumor cells to transit into CTC-like cells via upregulation of AST factors and related
152 mechanisms.
153

154 **Cell competition-derived in vitro CTC-like cells reflect in vivo CTC characteristics**

155 Next, we asked whether cell competition-derived *in vitro* CTC-like cells recapitulate *in vivo* CTCs
156 disseminated from primary tumors in mouse models. To test this, we integrated scRNA-seq data
157 obtained from parental and cell competition-derived CTC-like cells *in vitro* using the LM2 cell

158 line, a derivative of MDA-MB-231 cells that efficiently forms lung metastasis, and compared it
159 with scRNA-seq results from mouse tissue and liquid biopsy specimens that consist of
160 orthotopically injected LM2-derived primary tumors and CTCs collected from a fat pad-to-lung
161 metastasis model (**Fig. 2A**).

162 In UMAP analysis, LM2 cells harvested from *in vitro* cell competition assay and *in vivo*
163 mouse tissues were clustered into 4 groups (**Fig. 2B**). Surprisingly, we found that a portion of *in*
164 *vivo* CTCs were clustered adjacent to the *in vitro* CTC-like cells and shared similar transcriptomic
165 profiles based on Leiden algorithm (**Fig. 2C**). While most *in vivo* CTCs were located in Leiden
166 cluster 3, a subpopulation of CTCs with significantly high AST score, which measures the
167 expression level of AST factors, were grouped together with the CTC-like cell population in
168 Leiden cluster 1 (**Fig. 2D-E**). This result suggests that the expression of AST factors may drive
169 the transcriptomic similarities between *in vivo* CTCs and cell competition-derived CTC-like cells.
170 Thus, among the in vivo CTCs harvested from mouse metastasis model, we annotated these cells
171 as AST^{high} CTCs and investigated their characteristics compared to other groups (**Fig. 2F)**.
172 Surprisingly, Pearson correlation analysis revealed that the transcriptome of *in vivo* AST^{high} CTCs
173 exhibit the highest positive correlation with *in vitro* CTC-like cells, which was even stronger than
174 their primary tumor counterparts (**Fig. 2G)**. GSEA analyses indicate AST^{high} CTCs exhibit
175 impaired substrate adhesion, cell spreading, and Hippo signaling, which are hallmarks of CTCs in
176 mouse models and patients (**Fig. 2H)**. Notably, AST^{high} CTCs and CTC-like cells shared common
177 gene signatures related to downregulation of cell cycle, which resembles a feature of metastasis-
178 initiating cells that enter slow-cycling states for dormancy to survive the stresses of metasatic
179 processes (**Fig. 2I-J)**. We further identified the top five genes strongly expressed in both CTC-
180 like cells and AST^{high} CTCs, including BTG2, RGS2, NFKBIZ, IRE5, and SGK1, which have

181 shared functional roles in stress-adaptive quiescence that promotes CTC survival in hostile niches
182 (**Fig. 2H-J)**. This result strongly demonstrates that CTC-like cells generated through cell
183 competition physiologically recapitulate disseminated CTCs from the primary tumor that have
184 undergone AST-mediated reprogramming (**Fig. 2M)**.
185

186 **Oscillatory dynamics of AST factors confer anchorage plasticity of CTCs**

187 Characterization of cell competition-induced CTCs provides the basis to further investigate the
188 significance of AST factor plasticity in mouse models and human patients. To examine the
189 anchorage plasticity of CTCs, the loser cells or CTC-like cells were subsequently replated after
190 dissemination assay. Surprisingly, we found that CTC-like cells lost their anchorage independence
191 and readily colonized the culture dish to resume proliferation as adherent cells. We refer to these
192 newly adherent cells as mets-like cells because they simulate the latent phase of metastasis where
193 CTCs regain adhesive properties to reattach to the distant organs (**Fig. 3A**). Surprisingly, the
194 spontaneously detached CTC-like cells showed a significant reduction in AST factor expression,
195 which promoted their spontaneous detachment as mets-like cells, having undergone the
196 suspension-to-adherent transition (SAT) (**Fig. 3B**). These results show that AST factor dynamics
197 in CTC-like cells undergoing from AST to SAT transition correlate with the anchorage plasticity
198 of solid tumor cells in a way that is quite distinct from the primary-like or met-like cells. Our
199 findings demonstrate AST factors as anchorage-dependent, mechanosensitive transcriptional
200 regulators, highlighting the need for further investigation into the molecular mechanisms by which
201 mechanical cues modulate their transcriptional activity in solid tumor cells.

202 Building on our prior findings that AST factor induction facilitates CTC dissemination, we
203 next investigated whether repression of AST factors is a prerequisite for the reattachment and

204 metastatic colonization of CTCs *in vivo*. To this end, we established CTC-like LM2 cells by stably
205 expressing the AST factors (**Fig. 3C**).[8] Unlike mock-transduced adherent control cells, LM2-AST
206 cells elicited spontaneous detachment and resistance to anoikis. To assess whether sustained AST
207 factor expression with impaired plasticity could hinder metastatic colonization, we performed tail
208 vein injections of LM2-control and LM2-AST cells into NOD/SCID gamma (NSG) mice and
209 monitored lung colonization (**Fig. 3D**). Remarkably, while LM2-control cells efficiently formed
210 lung metastases, constitutive expression of AST factors in LM2-AST cells significantly impaired
211 lung colonization and extended overall survival **(Fig. 3E–G)**. These findings suggest that while
212 AST factor induction promotes CTC dissemination, their subsequent repression is essential for the
213 successful metastatic colonization of CTCs. Collectively, our data indicate that the dynamic
214 oscillation of AST factors, transient induction termed AST during the primary-to-CTC transition
215 followed by repression termed SAT during the CTC-to-metastasis transition, is a critical
216 determinant of the metastatic cascade.

217 Next, we asked whether Adherent-to-Suspension Plasticity (ASP) represents a clinically
218 relevant mechanism that dynamically regulates the anchorage dependency of CTCs during the
219 metastatic cascade in patients. To assess the clinical relevance of ASP in human patients, we
220 prospectively recruited 10 newly diagnosed *de novo* metastatic breast cancer patients and collected
221 matched specimens of primary breast tumors, peripheral blood, and metastatic lesions from each
222 patient **(Table S1, Fig. 3H)**. This cohort represents one of the most comprehensive biobanks in
223 breast cancer integrating both tissue and liquid biopsy specimens from the same individuals,
224 offering invaluable opportunities to investigate metastatic progression at the single-cell level[1-4].

225 CTCs were enriched from whole blood using high-density microporous (HDM) chips via
226 size-based exclusion, and tissue-derived cells and CTCs were processed for single-cell RNA

227 sequencing (scRNA-seq) analysis[9]. We identified multiple major cell types, including epithelial
228 tumor cells, fibroblasts, mesenchymal stem cells, and various immune populations such as myeloid
229 and lymphoid subsets (**Fig.S2A-B**). Tumor cells were identified by co-expression of EPCAM and
230 breast cancer-specific cytokeratins (KRT5, KRT8, KRT9, KRT17, or KRT18). Importantly,
231 UMAP projection not only revealed patient- and tissue-specific clustering, but also highlighted a
232 central, mixed cluster comprising cells from multiple patients and compartments, in which the
233 majority of CTCs were located (**Fig.3I**). Strikingly, this central cluster exhibited elevated
234 expression of AST factors, including IKZF1, NFE2, and IRF8. Quantitative analysis revealed that
235 AST factor expression was significantly higher in CTCs compared to both primary and metastatic
236 tumor cells, with IKZF1 and IRF8 exceeding statistical thresholds **(Fig. 3J, Fig. S2C)**. Notably,
237 this increase was consistent across different breast cancer subtypes and metastatic organ sites,
238 supporting the clinical relevance of ASP as a conserved mechanism in CTC biology. These
239 findings establish the upregulation of AST factors as a hallmark of anchorage plasticity during
240 metastatic dissemination in human breast cancer.

241 Extending upon our previous gene set enrichment analysis (GSEA) comparing primary
242 tumors and CTCs, we observed a significant enrichment of focal adhesion and extracellular matrix
243 (ECM) organization pathways in tissue-derived tumor cells relative to CTCs (**Fig.3K**)[7].
244 Specifically, focal adhesion-related gene expression was markedly elevated in both primary and
245 metastatic tumor samples compared to CTCs, while ECM organization pathways were
246 predominantly enriched in metastatic lesions (**Fig. S2D**). In contrast, CTCs exhibited
247 downregulation of genes encoding ECM components, integrins, and EMT-related genes consistent
248 with their anchorage-independent phenotype. Concurrently, CTCs showed a significant
249 upregulation of hemoglobin genes HBA1 and HBA2, which have been implicated in neutralizing

250 reactive oxygen species (ROS) and promoting resistance to anoikis (**Fig. 3K**)[7]. These
251 transcriptomic changes in matched tissue and liquid biopsy specimens from metastatic cancer
252 patients support the model that AST factor dynamics regulate anchorage plasticity through
253 transcriptional reprogramming of integrin/ECM-associated pathways and oxidative stress defense
254 in patients. Collectively, out results demonstrate the clinical relevance and mechanisms of
255 Adherent-to-Suspension Plasticity (ASP) in mediating the anchorage dependance of CTCs in
256 metastasis.
257

258 **Adherent-suspension plasticity in metastatic breast cancer patients**

259 To characterize the transcriptional dynamics underlying CTC formation and their relationship with
260 solid tumor cells, we further analyzed scRNA-seq database on matched primary tumors, CTCs,
261 and metastatic lesions from patients with *de novo* metastatic breast cancer. We first conducted
262 pseudotime and UMAP projection analyses to visualize cell state transitions across the metastatic
263 cascade (**Fig. 4A**). While cells clustered based on tissue origin, cancer stage, and patient identity,
264 it is important to note that a distinct central region emerged, where primary, metastatic, and CTC
265 populations overlapped in pseudotime space (**Fig. 4B**). Based on gene expression similarity and
266 reduced transcriptomic variance, we identified eight clusters (9, 11, 12, 13, 15, 17, 20, and 24) that
267 define the central region, which comprised 8,823 solid tumor cells (3,695 primary and 5,128
268 metastatic) and 39 CTCs (**Fig. 4C-D, Fig. S3A-B**).

269 Next, we further analyzed the origin of these central region cells and observed that the
270 majority of CTCs were localized in this region, which shared the pseudotime trajectories with
271 primary and metastatic tumor cells (**Fig. 4D**). We then examined AST factor expression in cells
272 located within the central region. Surprisingly, AST-positive cells (AST^+), including CTCs and a
273 subset of solid tumor cells were enriched in this region (**Fig. 4E**). RNA velocity analysis further

274 supported this transitionary state, indicating dynamic transcriptional activity toward a suspension
275 phenotype (**Fig. 4F**). Pseudotime expression plots revealed the plasticity of AST factors such as
276 IKZF1 and IRF8, which were significantly upregulated in intermediate states that correspond to
277 the central region, compared to early and later stages. These findings are consistent with the
278 oscillatory dynamics of AST factors shown in dissemination assay-derived CTC-like cells (**Fig.**
279 **4G**). Moreover, these results suggest that the transcriptional profile of solid tumor cells from
280 primary and metastatic lesions within the central region resembles gene signatures of CTCs,
281 indicating an intermediate state, not yet fully transformed into CTCs.

282 To further dissect the molecular basis of anchorage plasticity during the metastatic cascade,
283 we compared CTCs with matched solid tumor cells within the central region and identified 1,223
284 CTC-specific and 59 solid tumor-specific genes (**Fig. 4H, S3C**). Gene ontology analysis revealed
285 that CTC-specific genes were strongly enriched in rRNA processing and ribosome biogenesis
286 pathways, consistent with the elevated protein synthesis required for survival and adaptation of
287 disseminated CTCs (**Fig. 4I**). Notably, hemoglobin genes such as HBA1, which provide
288 antioxidant defense and promote anoikis resistance, were markedly upregulated in CTCs (**Fig. 4J**).
289 In contrast, solid tumor–specific genes were enriched for pathways related to cell–matrix adhesion
290 and extracellular matrix (ECM) organization (**Fig. 4I**), reflecting their anchorage-dependent state.
291 Together, these results indicate that CTCs transcriptionally reprogram toward an anchorage-
292 independent phenotype, supported by ribosome biogenesis and oxidative stress resistance, whereas
293 solid tumor cells retain adhesion and ECM-related programs underscoring the role of AST factor-
294 driven anchorage plasticity in mediating the CTC transition.

295 Pseudotime analysis further delineated the emergence of CTC-like states within solid
296 tumor specimens by showing that while the majority of tumor cells lacked AST factor expression

297 (AST-negative), a subset located at pseudotime positions proximal to CTCs displayed robust AST
298 factor expression (AST-positive) (**Fig. 4E–F**). We conducted DEG analyses across both primary
299 and metastatic tumors to investigate the differences between AST-positive and AST-negative solid
300 tumor cells. This allowed us to identify 2,112 AST-positive-specific genes and 166 AST-negative-
301 specific genes in the primary tumors versus 1,284 AST-positive-specific genes and 213 AST-
302 negative-specific genes in the metastatic tumors (**Fig**. **4K**). Underscoring the similarity of the two
303 conditions, we found a considerable overlap of 997 AST-positive-specific genes and 45 AST-
304 negative-specific genes that were shared between the primary and metastatic tumors. A GO
305 analysis of these AST-positive-specific genes revealed enrichment in the MAPK- ERK1/2 cascade,
306 which is associated with antioxidant expression, anoikis resistance, and metalloproteinase-
307 mediated ECM degradation (**Fig**. **4L**) [10-13]. In the AST-positive cells, we also identified genes
308 related to extravasation, which suggests that, like CTCs, these cells possess increased invasive
309 properties. In contrast, GO analysis of the AST-negative-specific genes revealed enrichment in
310 pathways related to anchoring junctions, ECM, and focal adhesions, which promote cell adhesion
311 and structural integrity (**Fig**. **4L**). GSEA analysis confirmed that AST-negative cells in both
312 primary and metastatic tumors showed significant enrichment in gene sets related to tight junctions
313 and ECM organization (**Fig**. **4M**). This further supports the notion that AST-negative cells are
314 characterized by strong adhesion properties. In contrast, AST-positive cells, particularly in the
315 central region, co-expressed genes involved in the MAPK cascade, ERK1/2 cascade, and
316 extravasation. Thus, some solid tumor cells exhibit an expression pattern like that of CTCs,
317 indicating the presence of cells with CTC-like characteristics within the solid tumor population.
318 Finally, we analyzed RNA velocity to clarify the correlation of AST factor expression
319 dynamics with the expression of integrin/ECM-related, antioxidant-related, and EMT-related

genes (**Fig. 4F, S3D**). Although we found no correlation between AST factors and EMT-related genes, there was a correlation between EMT-related genes and ECM-related genes, which correlates with our previous study that AST is independent of EMT.

Discussion

Cell competition in tumors is a system that leverages the heterogeneity of cancer cells in stressful microenvironments, such as high cell density, to select for cells that contribute to tumor survival and progression. During this process, less fit cells either undergo apoptosis or detach from the existing colonies. Recent studies have indicated that cells with metastatic traits can lose their competitive advantage within primary tumors and detach. In our study, we found that cells detached from the primary tumor due to cell competition acquire anchorage independence via AST factors, and are transcriptionally similar to circulating tumor cells (CTCs) expressing AST factors. This suggests the potential for conducting in vitro studies on CTCs using cell competition assays with metastatic cells. Previous attempts have aimed to study CTCs at the molecular level in vitro, including efforts to establish ex vivo CTC cell lines from patient samples. Furthermore, suspension assays, which assess anchorage-independent growth, have been widely used to investigate the anoikis resistance of CTCs. However, because this assay use trypsinized cells, they cannot mimic the spontaneous process by which CTCs disseminate *in vivo*, nor can they generate the exceedingly rare population of CTC-like cells that can freely detach from adherent culture conditions. Therefore, the CTC-like cells identified through cell competition will shed light on the overall understanding of the mechanical modulation involved in the dissemination and survival of AST-associated CTCs, paving the way for the discovery of potential anti-metastatic agents.

342 Our study highlights the need to distinguish anti-metastatic strategies from traditional
343 cancer therapies that promote competitive cells towards a less fit direction within the primary
344 tumor's cell competition context. For instance, cancer therapies targeting Hippo pathway effector
345 proteins such as TEAD or YAP suppress tumor proliferation by inhibiting the competitive
346 advantage of YAP^{hi} or $TEAD^{hi}$ cells. However, based on our findings that less fit CTC-like cells
347 or CTCs dissociated from the parental population are $TEAD^{low}$, targeting TEAD could
348 inadvertently increase the less fit cell population, potentially promoting metastasis. Therefore,
349 anti-cancer therapies and anti-metastatic agents should be developed with a more nuanced
350 understanding of how shifts in the dominance between competitive and less fit cells in the context
351 of cell competition within primary tumors can influence tumorigenesis and metastasis, respectively.
352 This approach would ensure that anti-cancer therapies do not inadvertently promote metastasis,
353 and anti-metastatic agents do not compromise tumor progression.

354 We demonstrated that, while AST factors facilitate the initial detachment and anoikis
355 resistance of CTC-like cells, their downregulation is essential for the reattachment and successful
356 colonization of cancer cells at distant metastatic sites. This indicates that metastatic success
357 depends on the ability of cancer cells to adapt their anchorage dependency to each stage of
358 metastasis. Suspension characteristics mobilize CTCs into the bloodstream, whereas reattachment
359 and colony formation necessitate a reversion to adherent traits within the microenvironment of
360 secondary sites. These insights challenge the conventional understanding of metastasis as a linear
361 progression and instead propose a model in which anchorage plasticity plays a central role in
362 cancer cells to spread during metastasis. ASP thus represents a novel cellular plasticity mechanism
363 analogous to epithelial-mesenchymal plasticity (EMP), another well-established process that
364 facilitates metastasis, however, limited to the transition between two different adhesive cell types.

365 How cancer cells orchestrate ASP and EMP during each stage of the metastatic cascade warrants
366 further investigation.

367 Our findings underscore the pivotal role of ASP in the metastatic cascade, as demonstrated
368 by scRNA-seq analysis of paired samples from *de novo* metastatic breast cancer patients,
369 encompassing matched primary tumors, CTCs, and metastatic lesions. This dataset offers
370 invaluable insights into tumor progression, adaptability, and heterogeneity across metastatic stages
371 in individual patients. The aggregation of CTCs from different patients within the central region
372 of the UMAP signifies that CTCs exhibit similar transcriptomic profiles despite their origin.
373 Importantly, the significant expression of AST factors not only in CTCs but also in their
374 intermediate solid tumor counterparts from pseudotime analysis indicate that anchorage plasticity
375 from AST to SAT is an adaptive and continuous process throughout the metastatic cascade. The
376 consistency of these trends across tumor subtypes and metastatic locations underscores the broad
377 significance of AST factors as theragnostic biomarkers of metastasis. To elucidate the role of
378 tumor microenvironment as an upstream mediator of AST factors, the spatiotemporal expression
379 patterns of AST factors using matched longitudinal specimens warrants further investigation.

380 Our study provides the rationale for clinical implementation of therapeutic strategies that
381 target AST factors and related mechanisms. For example, therapies designed to inhibit the
382 transition from adherent-to-suspension states, referred to as anti-disseminating agents, could
383 potentially be used as neoadjuvant therapies or alone to impede the initial detachment of cancer
384 cells from the primary tumor, thereby reducing the number of CTCs and the likelihood of
385 metastatic spread. Conversely, strategies that prevent the reattachment of CTCs at secondary sites
386 could hinder metastatic colonization, offering a two-pronged approach to tackle metastasis. A
387 deeper exploration into the genetic and epigenetic regulation of AST factors could yield additional

388 mechanistic insights into ASP. Understanding how AST factors are modulated during different
389 stages of metastasis, and the interplay between ASP and other forms of cellular plasticity, such as
390 EMP, warrants further investigation to delineate how these processes collectively contribute to the
391 completion of metastasis.

392 Together, our findings highlight the unprecedented role of ASP in breast cancer metastasis.
393 ASP provides a novel theoretical basis in cancer metastasis and suggests AST factors as promising
394 therapeutic targets to tackle the metastatic spread of solid tumor cells. Clinically, moving beyond
395 the primary tumor-centric point-of-view, our data expand the prevailing cancer treatment paradigm
396 toward direct intervention within the metastatic processes. The availability of cell-based platforms
397 that measure ASP efficiency and multi-omics database of matched longitudinal patient samples
398 could facilitate future research opportunities, including individualized metastasis prediction
399 models, hence augmenting the potential for developing effective anti-metastatic therapies [14].

400

401 **METHODS**

402 **DNA constructs**

403 AST genes were tagged with V5 and subcloned into the pENTR4 vector (Addgene, 17425 and
404 17423) using standard molecular cloning techniques. The resulting subcloned vectors were then
405 recombined with the destination vector pLentiCMV (Addgene, 17293) using LR recombinase
406 (Invitrogen, 1179019), generating the final lentiviral expression vectors.

407

408 **Cell culture**

409 Cells were maintained in a 37 °C humidified incubator with 5% CO_2. HEK293T, MCF7, HS578T
410 and MDA-MB-231 cells were cultured in DMEM (Hyclone, SH30022.01). BT549 cells were

411 cultured in RPMI (Hyclone, SH30027.01). Culture media were supplemented with 10% FBS
412 (Hyclone, SV30207.02) and 1% penicillin/streptomycin (Invitrogen, 15140122).
413
414 **Cell competition assay**
415 Cell competition assays were performed using MDA-MB-231, MCF7, BT549, and HS578T cells,
416 with each cell line cultured in its own respective growth media. For the assay, the cells were seeded
417 on normal plates at 80% confluency on the first day and then maintained for 3 days without any
418 media changes. After 3 days, the cells surpass 100% confluency, resulting in very high cell density.
419 After the old media were replaced with fresh media, the cells were cultured for an additional 3
420 days at 100% confluency. We noticed MDA-MB-231 cells began to round up and detach from the
421 plate beginning on the second day after the media change. By the third day, we observed a higher
422 number of CTC-like cells. These detached CTC-like cells were harvested by collecting the media,
423 followed by centrifugation to isolate the cells. For MCF7 cells, despite the media change, the cells
424 began to die after 3 days. Although BT549 and HS578T cells did not exhibit cell death, they did
425 cease proliferating.
426
427 **Viral infection**
428 To generate lentiviral particles, HEK293T cells were transfected with plasmids encoding pMD2G
429 and psPAX2, along with the lentiviral vectors containing the desired constructs. Transfections
430 were performed using Polyplus Reagent (Merck) according to the manufacturer's protocol. At 48
431 hours post-transfection, media containing the viral particles were harvested from the transfected
432 cells. The harvested media were then filtered through a 0.45 μm filter to remove cellular debris.
433 To enhance infection efficiency, the filtered media were supplemented with 8 mg/ml polybrene.
434 The transduced cells were infected with the lentiviral particles by incubating them with the filtered

435 media. After 24 hours of infection, the media were changed, and the cells were incubated for
436 another 24 hours. Then, transduced cells were selected using puromycin. The selection process
437 allowed for the enrichment of cells that successfully integrated the lentiviral vectors and expressed
438 the desired genes or markers.
439
440 **Cell viability assay**
441 *In vitro* cell viability was assessed using the CellTiter Glo® 2.0 cell viability assay (Promega,
442 G9241) and the LIVE/DEAD® cell imaging kit (ThermoFisher, R37601) according to their
443 manufacturers' protocols. For the suspension assay, cells were plated on Corning® Costar® Ultra-
444 Low Attachment Multiple-Well Plates (Merck, CLS3471).
445
446 **Quantitative real-time PCR analysis**
447 Cellular RNA samples were collected via RNA extraction using the RNeasy Plus mini kit
448 (QIAGEN, 74136). These RNA samples were then reverse transcribed into complementary DNA
449 (cDNA) using iScript reverse transcriptase (Bio-Rad, 1708891). The KAPA SYBR FAST qPCR
450 kit (Kapa Biosystems, KK4605) and the 7300 real-time PCR system (Applied Biosystems) were
451 used for quantitative real-time PCR (qRT-PCR). The following primer sequences were used for
452 qPCR: IKZF1, 5'-TTTCAGGGAAGGAAAGCCCC-3' (forward) and 5'-
453 CTCCGCACATTCTTCCCCAT-3' (reverse); NFE2, 5'-ACAGCTGTCCACTTCAGAGC-3'
454 (forward) and 5'-TGAGCAGGGGCAGTAAGTTG-3' (reverse); IRF8, 5'-
455 AGCATGTTCCGGATCCCTTG-3' (forward) and 5'-CGGTCCGTCACTTCCTCAAA-3'
456 (reverse); and ACTB, 5'-GCCGACAGGATGCAGAAGGAGATCA-3'(forward) and 5'-
457 AAGCATTTGCGGTGGACGATGGA-3'(reverse).
458

459 **siRNA transfection**

460 A transfection mix was prepared by combining 100 µl of Opti-MEM™ medium (ThermoFisher,
461 #31985070), 12 µl of RNAi Max transfection reagent (Invitrogen, 13778150), and 2 µl of 20 µM
462 siRNA. The following siRNAs were used for transfection: non-silencing (NS) siRNA (Dharmacon
463 siGENOME non-targeting control pool #D-001206-13-200), siIKZF1 (Dharmacon siGENOME
464 SMARTPool #M-019092-01-0010), siNFE2 (Dharmacon siGENOME SMARTPool #M-010049-
465 00-0010), siIRF8 (Dharmacon siGENOME SMARTPool #M-011699-01-0010), and siPOU2F2
466 (Dharmacon siGENOME SMARTPool #M-019690-01-0010).

467

468 **Mouse model experiments**

469 All animal experiment protocols in this study underwent a thorough review and received approval
470 from the Yonsei University Institutional Animal Care and Use Committee (IACUC). All
471 procedures involving animals adhered to the Guidelines for the Care and Use of Laboratory
472 Animals. The NOD SCID Gamma (NSG) mice used for orthotopic injection experiments were
473 obtained from JA Bio. For the orthotopic mouse model experiments, mammary fat pads of 7-week-
474 old female NSG mice were orthotopically injected with $1x10^6$ MCF7, BT549, HS578T, or MDA-
475 MB-231 cells. For the mouse tail vein injection experiments, the tail veins of 7-week-old female
476 NSG mice were injected with $1x10^5$ MDA-MB-231 derivative LM2 cells. At week 4, the mice
477 were euthanized for bioluminescence imaging using the In Vivo Imaging Spectrum (IVIS) device
478 (PerkinElmer, CLS136331 IVIS Lumina LT Inst, Series III, 120 V). All *in vivo* experiments were
479 carried out using mice that had received the same treatment. The NSG mice used in these
480 experiments possessed an identical genotype and genetic background.

481

482 **Statistical analyses**

483 All quantitative data were obtained from at least three independent biological replicates. Data are
484 presented as means ± standard deviation (SD) unless otherwise noted in the figure legends.
485 Statistical differences between two groups were examined using two-tailed, unpaired Student's t-
486 tests or one-way analysis of variance (ANOVA) with Bonferroni corrections for multiple
487 comparisons. Statistical tests were performed using the GraphPad Prism 9.0 software (GraphPad
488 Software, CA, USA). Two-sided p-values of less than 0.05 were considered significant. No
489 statistical methods were used to predetermine sample size. Sample size was based on previous
490 experience with experimental variability. Blinding was performed wherever possible during all
491 sample analysis by coding sample identity during data collection and having the analysis
492 performed by an observer without knowledge of or access to the experimental conditions.
493

494 **Bioinformatics of primary tumor cells, CTCs, and metastatic cancer cells**

495 The illumina outputs for human samples were mapped to the human reference genome (GRCh38)
496 using Cell Ranger 7.1.0 (10X Genomics). Gene-wise read counts for genes with at least 500 reads
497 were exported from Cell Ranger to the Matrix Market format and imported into R with Seurat's
498 Read10X function. An average of > 135 million reads from > 13,000 cells were obtained for each
499 sample. Each 10X library was individually checked for quality, and the cells were filtered
500 according to the same criteria used in our previous study to ensure good gene coverage [7]. After
501 quality control filtering, a total of 310,189 cells remained, with 69,612 cells from the primary
502 tumor site, 171,504 cells from the blood, and 79,073 cells from the metastatic site (**Table 1**).
503 Samples were combined via an algorithm implemented in Seurat. The default Seurat function
504 settings were used, and 1:20 principal component dimensions were used for all dimension
505 reduction and integration steps. The cluster resolutions were set to 0.5, unless otherwise stated.

506 The RunUMAP random seed was set to 1,000 to ensure reproducibility. Marker genes for cell
507 clusters were identified using Seurat's FindMarkers function with the default settings. Cell type
508 annotation was performed using the SingleR package (v2.6.0) with the HumanProteinAtlas
509 database from the celldex package (v1.14.0). Cells co-expressing EPCAM and cytokeratins such
510 as KRT5, KRT8, KRT9, KRT17, or KRT18 were designated as cancer cells. A total of 54,867
511 cells were used for the analysis, including 26,227 cells from the primary tumor site, 50 cells from
512 the blood, and 28,590 cells from metastatic sites (**Table 1**). The cells designated as cancer cells
513 were subsequently extracted and reanalyzed beginning with the normalization process. DEGs were
514 selected with thresholds for the FDR corrected p-value < 0.001 and an absolute $\log_2$ fold change
515 ≥ 1. GO analysis was performed using the gseGO function from clusterProfiler (v3.0.4). GSEA
516 plots were generated from the DEG data using the gseaplot function. Pseudotime analysis was
517 performed using the monocle package (v3.0) with normalized data, UMAP coordinates, and cluster
518 information obtained from the initial Seurat analysis. The calculation of gene set scores along
519 pseudotime was conducted for each cell using the AddModuleScore function in Seurat. All plots
520 were exported to the PDF format using R and their dimensions were adjusted in Illustrator.
521
522
523
524
525
526
527
528

Declarations

Ethical approval

Ethical approval for the use of human subjects was obtained from the Institutional Review Board of Gangnam Severance Hospital, Yonsei University, Seoul, Republic of Korea (3-2021-0236) in compliance with the ethical guidelines of the 1975 Declaration of Helsinki, and informed written consent was obtained from each patient. Collection of human breast cancer samples were obtained from consenting patients in accordance with guidelines and regulations approved by the Institutional Review Board of Gangnam Severance Hospital, Yonsei University Health System (3-2021-0236). The animal experiment protocols were reviewed and approved by the Yonsei University Institutional Animal Care and Use Committee (IACUC).

552 **Competing interests**

553 The authors declare that they have no conflict of interest.

554

555 **Fundings and acknowledgments**

556 This work was supported by grants from the National Research Foundation of Korea (RS-2024-
557 00509461 to H.W.P), by the Brain Korea 21 FOUR Program (to H.D.H., Y.S., H.L., B.J.H.,
558 W.Y.P., J.O., and D.K.L.)

559

560 **Authors' contributions**

561 H.D.H., Y.S., and J.H.K. performed most of the experiments. H.L., B.J.H., W.Y.P. performed drug
562 treatment and imaging. J.O., and D.K.L. performed transcriptome analyses. S.P. and J.C.
563 performed CTC isolation and scRNAseq. J.J., H.Y.G., and H.W.P. designed the study and wrote
564 the manuscript.

565 **References**

566 1. Koch, C., Kuske, A., Joosse, S.A., Yigit, G., Sflomos, G., Thaler, S., Smit, D.J.,
567 Werner, S., Borgmann, K., Gartner, S., et al. (2020). Characterization of circulating
568 breast cancer cells with tumorigenic and metastatic capacity. EMBO Mol Med *12*,
569 e11908. 10.15252/emmm.201911908.

570 2. Sun, Y.F., Wu, L., Liu, S.P., Jiang, M.M., Hu, B., Zhou, K.Q., Guo, W., Xu, Y., Zhong,
571 Y., Zhou, X.R., et al. (2021). Dissecting spatial heterogeneity and the immune-
572 evasion mechanism of CTCs by single-cell RNA-seq in hepatocellular carcinoma.
573 Nat Commun *12*, 4091. 10.1038/s41467-021-24386-0.

574 3. Ebright, R.Y., Lee, S., Wittner, B.S., Niederhoffer, K.L., Nicholson, B.T., Bardia, A.,
575 Truesdell, S., Wiley, D.F., Wesley, B., Li, S., et al. (2020). Deregulation of ribosomal
576 protein expression and translation promotes breast cancer metastasis. Science *367*,
577 1468-1473. 10.1126/science.aay0939.

578 4. Garcia-Recio, S., Hinoue, T., Wheeler, G.L., Kelly, B.J., Garrido-Castro, A.C.,
579 Pascual, T., De Cubas, A.A., Xia, Y., Felsheim, B.M., McClure, M.B., et al. (2023).
580 Multiomics in primary and metastatic breast tumors from the AURORA US
581 network finds microenvironment and epigenetic drivers of metastasis. Nat Cancer
582 *4*, 128-147. 10.1038/s43018-022-00491-x.

583 5. Turajlic, S., Xu, H., Litchfield, K., Rowan, A., Chambers, T., Lopez, J.I., Nicol, D.,
584 O'Brien, T., Larkin, J., Horswell, S., et al. (2018). Tracking Cancer Evolution Reveals
585 Constrained Routes to Metastases: TRACERx Renal. Cell *173*, 581-594 e512.
586 10.1016/j.cell.2018.03.057.

587 6. Jin, X., Demere, Z., Nair, K., Ali, A., Ferraro, G.B., Natoli, T., Deik, A., Petronio, L.,
588 Tang, A.A., Zhu, C., et al. (2020). A metastasis map of human cancer cell lines.
589 Nature *588*, 331-336. 10.1038/s41586-020-2969-2.
590 7. Huh, H.D., Sub, Y., Oh, J., Kim, Y.E., Lee, J.Y., Kim, H.R., Lee, S., Lee, H., Pak, S.,
591 Amos, S.E., et al. (2023). Reprogramming anchorage dependency by adherent-to-
592 suspension transition promotes metastatic dissemination. Mol Cancer *22*, 63.
593 10.1186/s12943-023-01753-7.
594 8. Minn, A.J., Gupta, G.P., Siegel, P.M., Bos, P.D., Shu, W., Giri, D.D., Viale, A.,
595 Olshen, A.B., Gerald, W.L., and Massague, J. (2005). Genes that mediate breast
596 cancer metastasis to lung. Nature *436*, 518-524. 10.1038/nature03799.
597 9. Lee, S.J., Lee, C.H., Choi, S.H., Ahn, S.H., Son, B.H., Lee, J.W., Yu, J.H., Kwon, N.J.,
598 Lee, W.C., Yang, K.S., et al. (2017). Evaluation of a novel approach to circulating
599 tumor cell isolation for cancer gene panel analysis in patients with breast cancer.
600 Oncol Lett *13*, 3025-3031. 10.3892/ol.2017.5807.
601 10. Li, F., Liang, H., You, H., Xiao, J., Xia, H., Chen, X., Huang, M., Cheng, Z., Yang,
602 C., Liu, W., et al. (2022). Targeting HECTD3-IKKα axis inhibits inflammation-
603 related metastasis. Signal Transduct Target Ther *7*, 264. 10.1038/s41392-022-01057-
604 0.
605 11. Yuan, S., Norgard, R.J., and Stanger, B.Z. (2019). Cellular Plasticity in Cancer.
606 Cancer Discov *9*, 837-851. 10.1158/2159-8290.CD-19-0015.
607 12. Fanelli, G.N., Naccarato, A.G., and Scatena, C. (2020). Recent Advances in Cancer
608 Plasticity: Cellular Mechanisms, Surveillance Strategies, and Therapeutic
609 Optimization. Front Oncol *10*, 569. 10.3389/fonc.2020.00569.

610 13. Akhmetkaliyev, A., Alibrahim, N., Shafiee, D., and Tulchinsky, E. (2023).
611 EMT/MET plasticity in cancer and Go-or-Grow decisions in quiescence: the two
612 sides of the same coin? Mol Cancer *22*, 90. 10.1186/s12943-023-01793-z.
613 14. Anderson, R.L., Balasas, T., Callaghan, J., Coombes, R.C., Evans, J., Hall, J.A.,
614 Kinrade, S., Jones, D., Jones, P.S., Jones, R., et al. (2019). A framework for the
615 development of effective anti-metastatic agents. Nat Rev Clin Oncol *16*, 185-204.
616 10.1038/s41571-018-0134-8.
617

Figure 1. Cell competiton orchestrates spontaneous detachment of CTC-like cells driven by AST factors expression *in vitro*

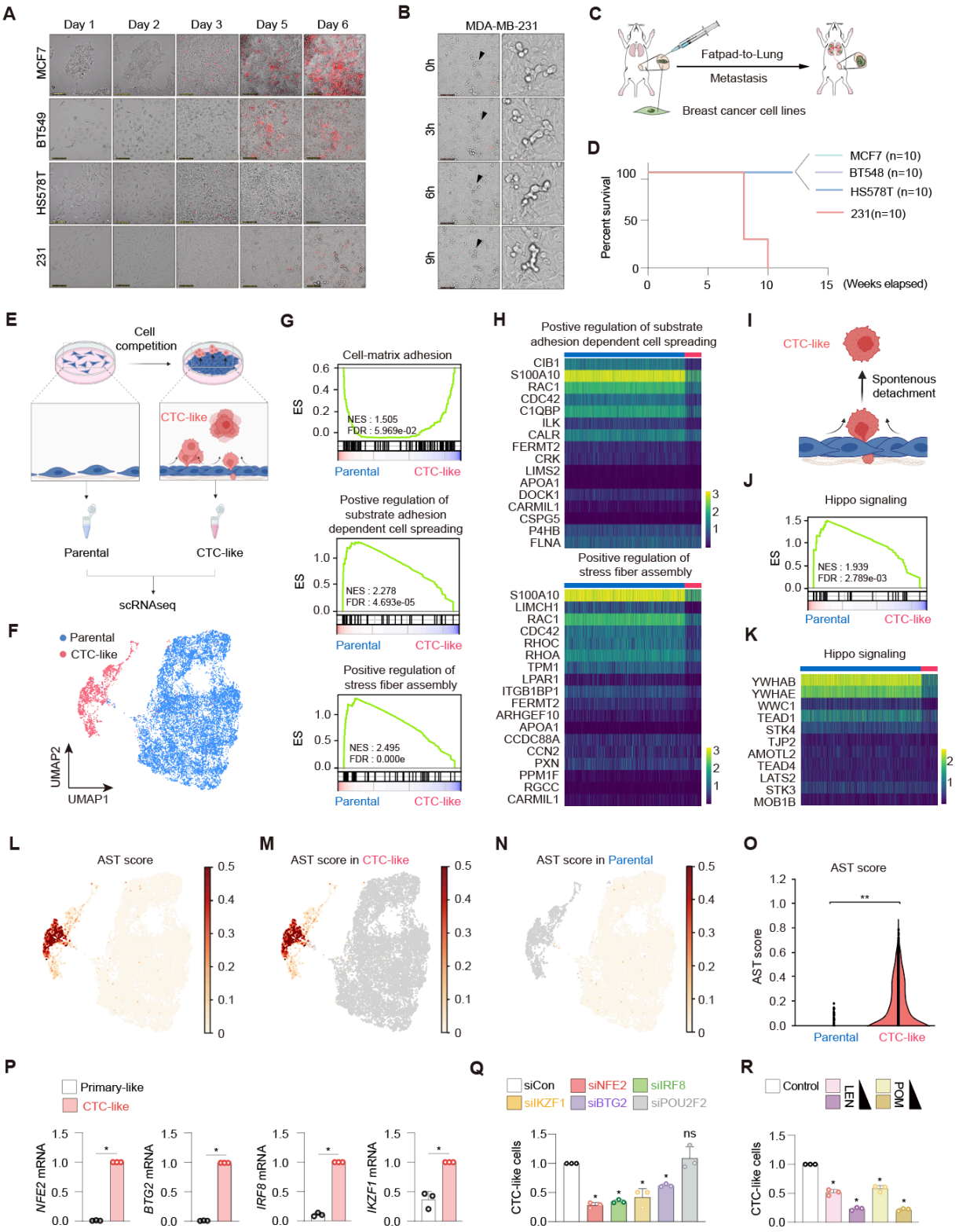

621 **A**, Representative fluorescence images MCF7, BT549, Hs578T and MDA-MB-231 cells stained
622 for viability with propidium iodide. Red, dead. Scale bars, 100 μm. **B**, Time-lapse microscopy
623 images showing spontaneous cell detachment of MDA-MB-231 cells in the dissemination assay.
624 **C**, Schematic overview of mammary fat pad xenografts of 4 different breast cancer cell lines. **D**,
625 Kaplan-Meier survival plot showing the survival rates of mice injected with MCF7, BT549,
626 Hs578T, or MDA-MB-231 cells. **E**, Schematic overview of the isolation and scRNA-seq analysis
627 of parental cells and circulating tumor cells-like (CTC-like) cells from cell competition. **F**,
628 Uniform manifold approximation and projection (UMAP) of scRNA-seq cells (13,918 cells)
629 colored by parnetal (blue) and CTC-like cells (red). **G**, Gene set enrichment analysis (GSEA)
630 results for cell-matrix adhesion, positive regulation of substrate adhesion dependent cell spreading,
631 and positive regulation of stress fiber assembly gene sets within CTC-like cells. **H**, Heatmap
632 showing differentially expressed genes (DEGs). DEGs were identified based on gene set enriched
633 in GSEA result in (G). **I**, Schematic overview of spontaneously detached CTC-like cells from
634 parental cells. **J**, Gene set enrichment analysis (GSEA) results for hippo signaling gene sets within
635 CTC-like cells. **K**, Heatmap showing differentially expressed genes (DEGs). DEGs were identified
636 based on gene set enriched in GSEA result in (K). **L**, UMAP of scRNA-seq cells showing AST
637 score, calculated with Scnapy's score_genes function, which reflects the normalized difference in
638 mean expression between AST genes (IKZF1, NFE2, BTG2, and IRF8) and control genes. **M**,
639 UMAP of scRNA-seq cells showing AST score in CTC-like cells. **N**, UMAP of scRNA-seq cells
640 showing AST score in parental cells. **P,** Representative images of CTC-like MDA-MB-231 cell
641 morphology and quantitative real-time PCR analysis of AST factor transcript levels in CTC-like
642 cells. **Q**, The number of CTC-like cells for MDA-MB-231 cells following siRNA-mediated AST

643 factor depletion. N = 3. **R**, The number of CTC-like cells for MDA-MB-231 cells following
644 treatment with lenalidomide or pomalidomide. N = 3.
645
646
647
648
649
650
651
652
653
654
655
656
657
658
659
660
661
662
663
664
665

666

667 **Figure 2. CTC-like cells reflect CTCs characterized by AST factor expression.**

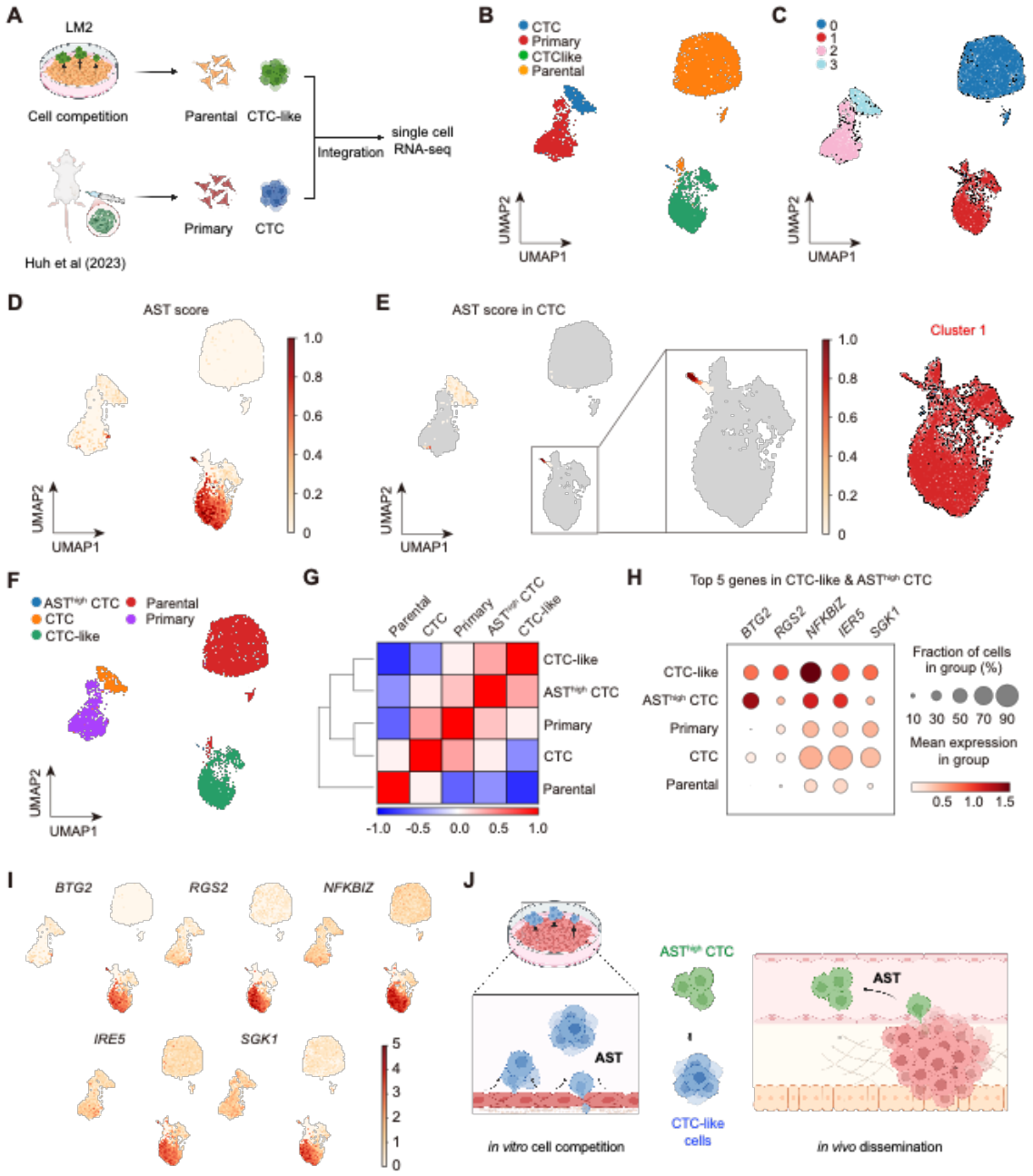

668

669 **A,** Schematic overview illustrating the integration of scRNA-seq analysis of in vitro cell

670 competition data (parental cells and CTC-like cells) with in vivo orthotopic fatpad-to-lung

671 metastasis data (primary tumor and circulating tumor cells, CTCs). **B**, Uniform manifold
672 approximation and projection (UMAP) of scRNA-seq cells (26,571 cells) colored by samples
673 (CTCs, primary tumor, CTC-like cells and parental cells) **C**, Uniform manifold approximation and
674 projection (UMAP) of scRNA-seq cells (26,571 cells) colored by leiden algorithm. **D**, Uniform
675 manifold approximation and projection (UMAP) of scRNA-seq cells (26,571 cells) colored by
676 normalized AST score, calculated with Scnapy's score_genes function, which reflects the
677 normalized difference in mean expression between AST genes (IKZF1, NFE2, BTG2, and IRF8)
678 and control genes. **E**, Uniform manifold approximation and projection (UMAP) of scRNA-seq
679 cells (26,571 cells) colored by normalized AST score in CTCs. **F**, Uniform manifold
680 approximation and projection (UMAP) of scRNA-seq cells (26,571 cells) colored by annotated
681 cell type (AST^{high} CTCs, CTC-like, CTCs, primary tumor, and parental cells). **G**, Pearson
682 correlation analysis showing the transcriptional correation between annotated cell types in **F**. **H**,
683 Dot plots showing the expression level of five top genes that is highly expressed in AST^{high} CTCs
684 and CTC-like in annotated cell types in **F**. **I**, Uniform manifold approximation and projection
685 (UMAP) of scRNA-seq cells (26,571 cells) colored by normalized expression of 5 top genes in **H**.
686 **J**, Schematic model illustrating that in vitro CTC-like cells generated thorugh cell competition
687 recapitulate in vivo AST^{high} CTCs.
688
689
690
691
692
693
694

Figure 3. CTC-like cells and CTCs confer anchorage dependency plasticity accompanied by AST factors oscillation.

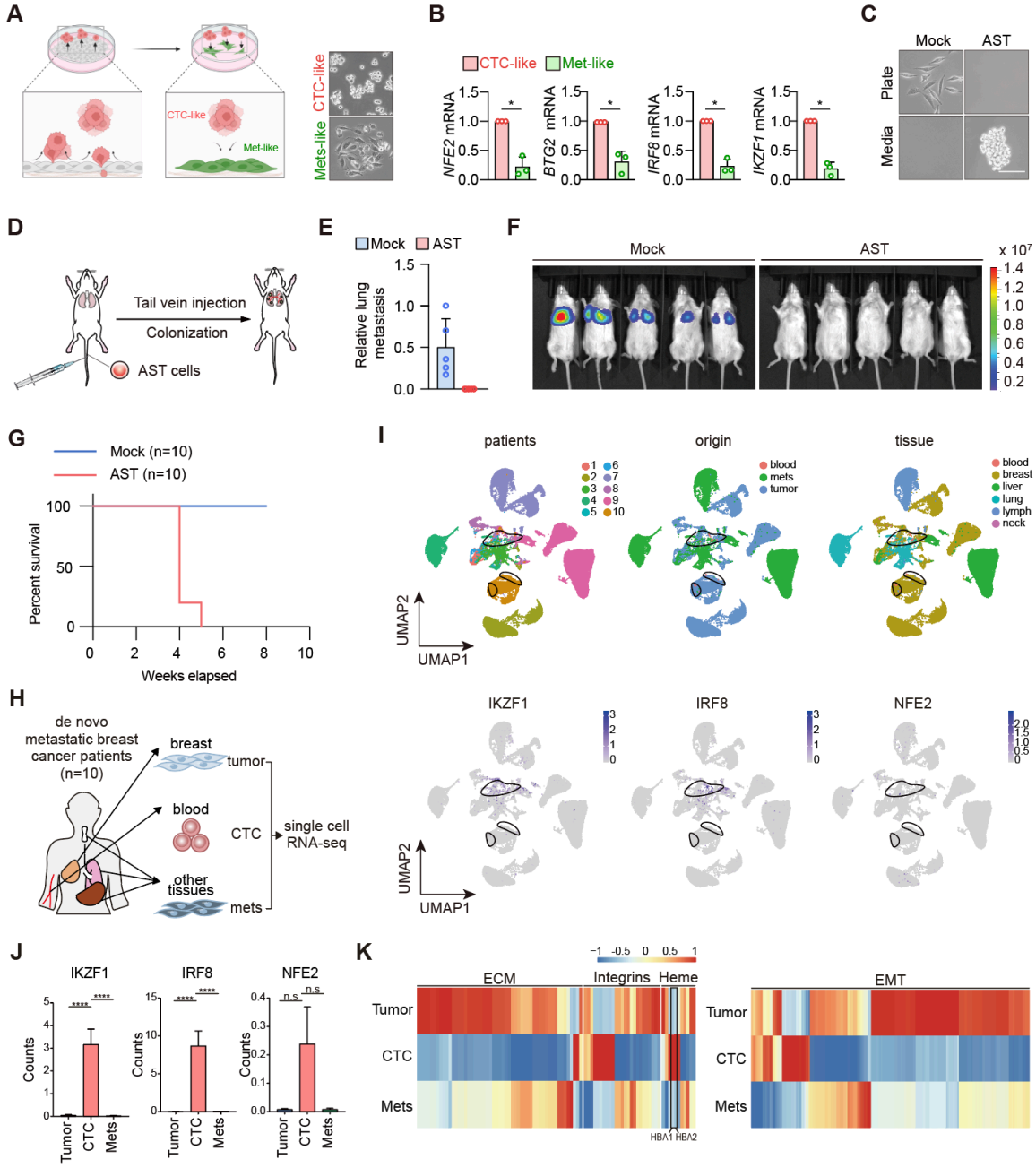

A, Schematic overview of CTC-like cells and mets-like cells, and representative images of re-attached MDA-MB-231 cell (met-like cells) morphology. **B**, Quantitative real-time PCR analysis of AST factor transcript levels in met-like cells compared to CTC-like cells. **C**, Representative

701 images of MDA-MB-231 derivates LM2-mock or AST cell (LM2 cells expressing AST factors)
702 morphology on a culture plate or in media. **D**, Schematic overview of tail vein injections with
703 LM2-mock or AST cells. **E**, Bioluminescence images of lung metastases after LM2 tail vein
704 injections. **F**, Lung metastases quantified by lung bioluminescence intensity for mock versus AST
705 cells. **G**, Kaplan-Meier survival plot showing the survival rates of mice injected with mock or
706 3AST cells. N = 10. **H,** Schematic overview of the isolation and scRNA-seq analysis of primary
707 tumor cells, circulating tumor cells (CTCs), and metastatic tumor cells from de novo metastatic
708 breast cancer patients (n = 10). CTCs were isolated using HDM chips. **I,** Uniform manifold
709 approximation and projection (UMAP) of scRNA-seq cells (n = 10; 54,866 cells) colored by
710 patient, origin, tissue, and normalized gene expression of the AST factors IKZF1, IRF8, and NFE2.
711 Black border lines, area in which the CTCs are located. **J,** Dynamite plots showing the expression
712 of (left) IKZF1, (middle) IRF8, and (right) NFE2 in primary tumor cells, CTCs, and metastatic
713 tumor cells. ****, $P < 0.0001$; n.s, not significant ($P > 0.05$). **K**, Heatmaps showing normalized
714 expression of four gene sets—ECM, integrins, antioxidant defense genes, and EMT-related
715 genes—in primary tumors, CTCs, and metastases. The average normalized expression values for
716 cells within each group are displayed as scaled values. Black-bordered box, HBA1 and HBA2.
717

718 **Figure 4. AST plasticity in matched single cell RNA-seq samples from *de novo* breast**

719 **cancer patients.**

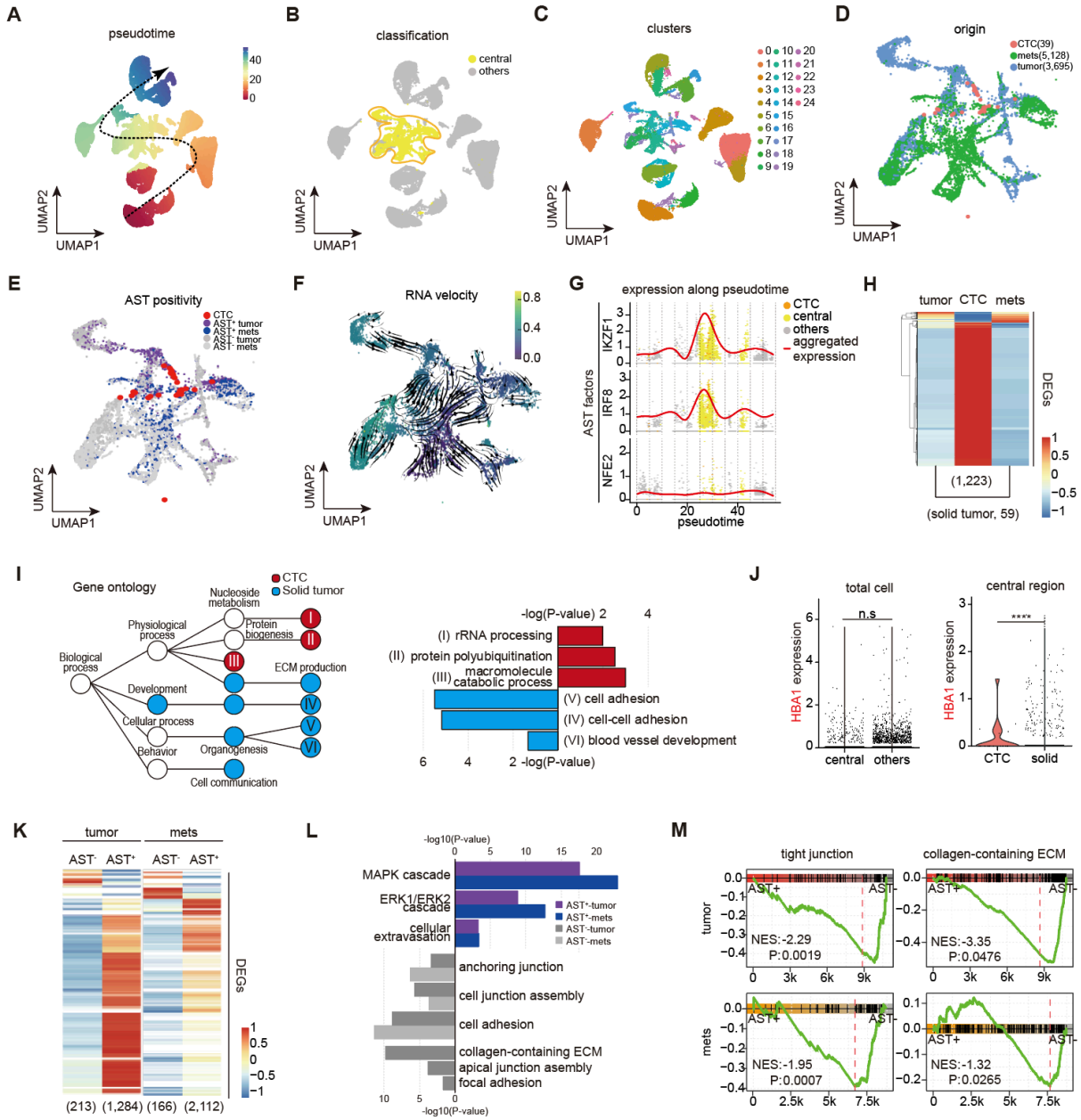

720

721 **A-C**, UMAP plot showing pseudotime (A), a division between the central region containing

722 complex clusters with CTCs and others (B), and clusters calculated at a resolution of 0.5 (C).

723 Dotted arrow, flow of pseudotime for the normalized gene expression of the AST factors IKZF1,

724 IRF8, and NFE2. **D-F**, UMAP of the central region colored according to origin (D) , AST positivity

725 (E), and RNA velocity (F). **G**, Pseudotime expression plots showing AST factors. X-axis,
726 pseudotime; y-axis, expression levels; gray dots, others; yellow dots, central region; orange dots,
727 CTCs; red line, linear expression trend using generalized additive modeling (GAM). **H**, Heatmap
728 showing differentially expressed genes (DEGs). DEGs were identified based on comparisons
729 between solid tumor cells and CTCs within the central region and selected with a threshold p-value
730 < 0.05. There were 1,223 CTC DEGs and 59 solid tumor DEGs. **I**, Gene ontology tree showing
731 the CTC-specific gene set and the solid tumor-specific gene set with a bar plot showing the gene
732 names and the p-values corresponding to the circles marked with roman numerals. Colored circles,
733 statistically significant, FDR corrected $P < 0.01$. **J**, Violin plots with dots showing HBA1
734 expression. The first plot compares the central region with other groups, while the second plot
735 compares CTCs with solid tumor cells within the central region. Yellow, central region; gray,
736 others; orange, CTCs within the central region; turquoise, solid tumor cells within the central
737 region; ****, $P < 0.0001$; n.s, not significant ($P > 0.05$). **K**, Heatmap showing DEGs. In a
738 comparison of cells with and without AST factor expression in both primary and metastatic tumors,
739 the DEG thresholds were defined as an FDR corrected q-value < 0.001 and an absolute fold change
740 > 2. **L**, Bar plot showing ontology analysis results for the AST-positive and AST-negative gene
741 sets identified in (**K**). Purple bars, AST-positive gene sets in primary tumors; blue bars, AST-
742 positive gene sets in metastatic tumors; gray bars, AST-negative gene sets in primary tumors; light
743 gray bars, AST-negative gene sets in metastatic tumors. **M**, Gene set enrichment analysis (GSEA)
744 results for tight junction and collagen-containing ECM gene sets within both primary and
745 metastatic tumors.
746
747

748 **Supplementary Figure 1. The ability to generate AST factors-expressing CTC-like cells is**

749 **correlated with their metastatic capability.**

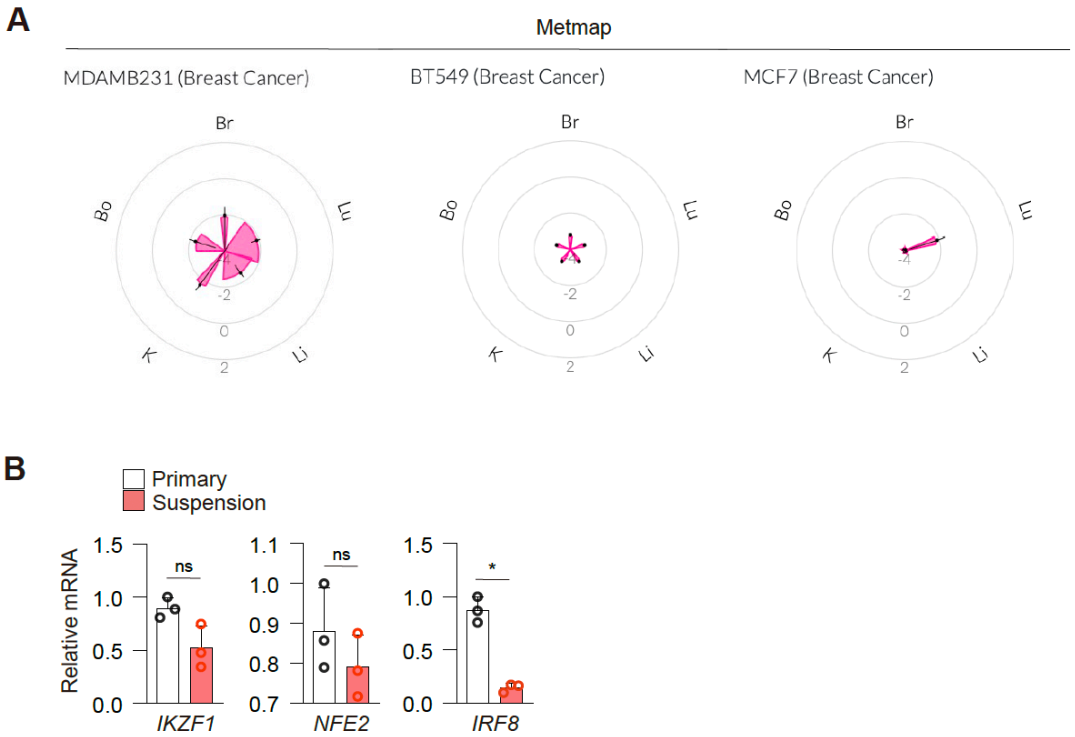

750

751 **A**, Petal plots showing the metastatic patterns of 3 breast cancer cell lines. Data for these plots

752 were obtained from Jin, X., *et al*. (https://depmap.org/metmap). **B**, Quantitative real-time PCR

753 analysis of AST factor transcript levels in cells harvested from suspension assay.

754 **Supplementary Figure 2. Comprehensive overview of single cell RNA sequencing**

755 **data from breast cancer patients.**

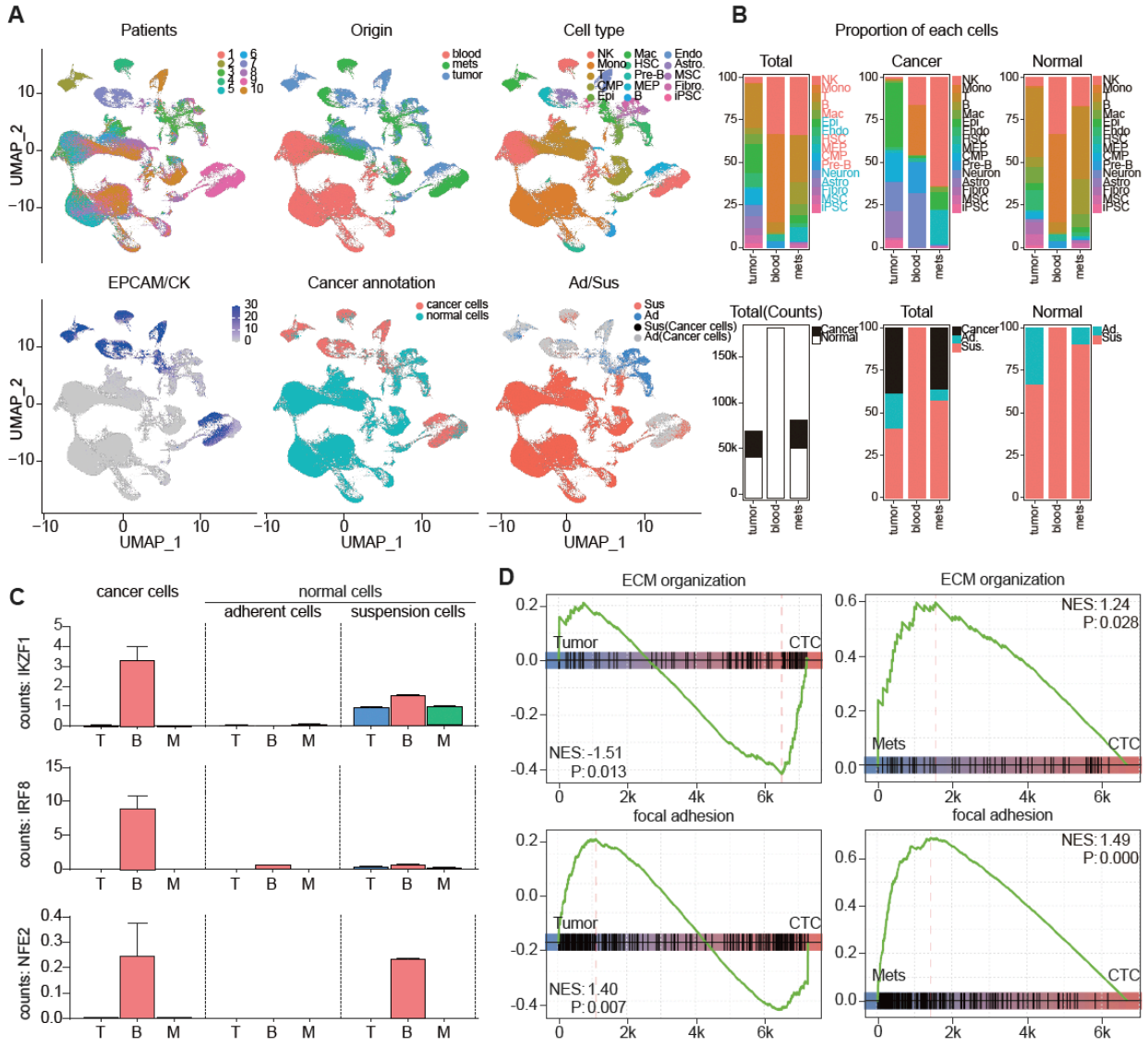

756

757 **A**, Uniform manifold approximation and projection (UMAP) of scRNA-seq cells (n = 316,539

758 cells) colored by patient, origin, cell type, normalized gene expression of cancer cell markers

759 (EPCAM, KRT5, KRT7, KRT8, KRT18, and KRT19), cancer/non-cancer annotation, and the

760 combined cancer/non-cancer and adherent/suspension annotation. **B**, Bar plots showing a

761 breakdown of cell type composition across tumor, blood, and metastasis samples. The first row

762 shows the proportion of various cell types in total cells, cancer cells, and normal cells. The
763 second row shows the proportion of cancer cells versus normal cells, adherent versus suspension
764 cells within cancer and normal cells, and adherent versus suspension cells within normal cells. **C**,
765 Dynamite plots depicting the expression of the AST factors IKZF1, IRF8, and NFE2 in cancer
766 cells from primary tumor, blood, and metastases, as well as normal cells split into adherent and
767 suspension states. **D**, Gene set enrichment analysis (GSEA) plots for focal adhesion and ECM
768 organization gene sets comparing CTCs to primary tumor or metastatic cells.

Supplementary Figure 3. Central region-specific cell populations and CTC–solid tumor divergence in scRNA sequencing data.

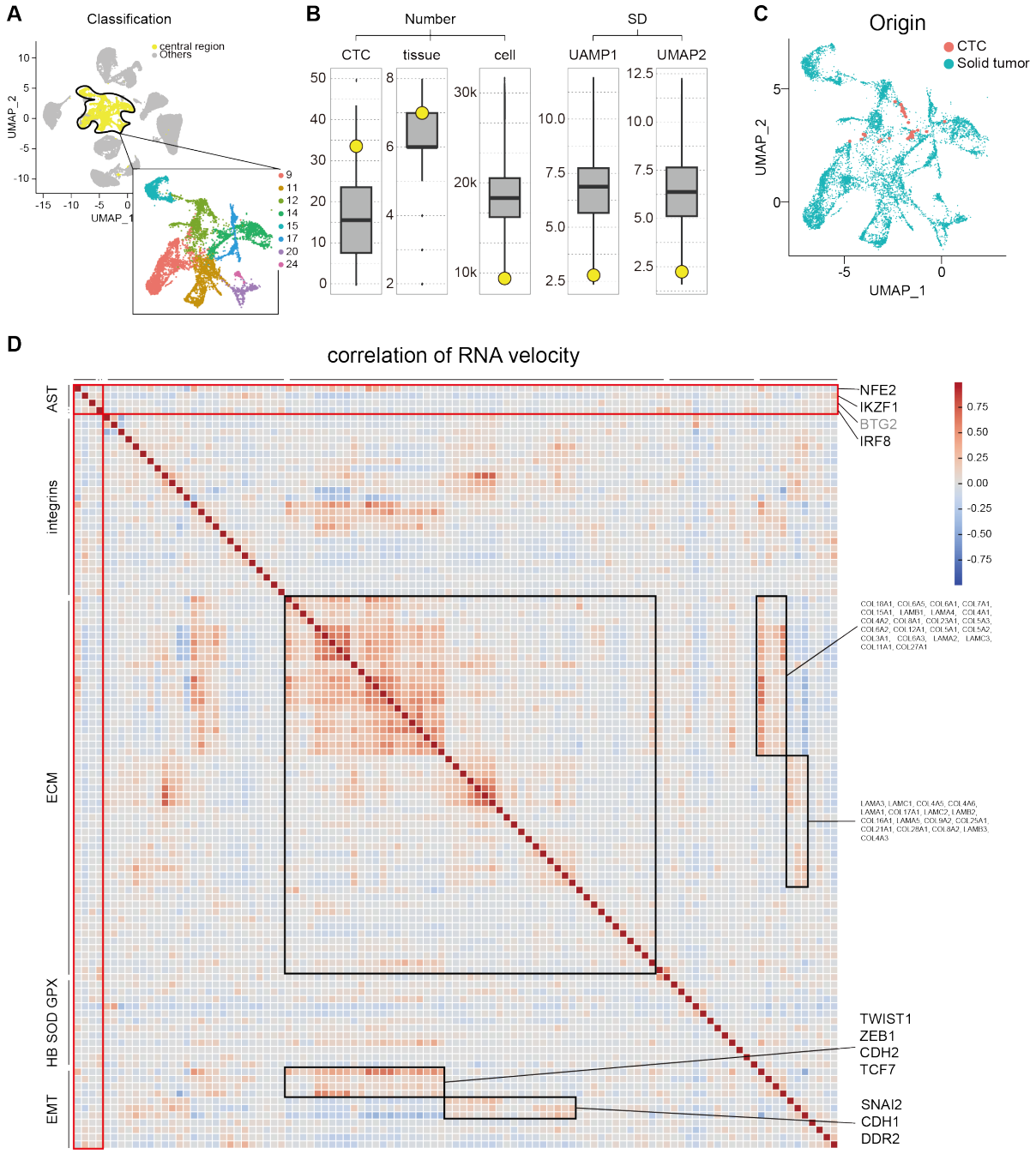

A, UMAP of cancer cells categorized into the central region and others. A magnified view of the central region is also shown to highlight its specific clusters. **B**, Boxplots of 1,081,575 cluster

775 combinations (binomial coefficient with n = 25, k-permutation = 8) presenting numbers of CTCs,
776 originating tissues, and total cells with standard deviations (SDs) for UMAP1 and UMAP2. Yellow
777 dot, selected cluster combination; CTCs, n = 34, 11.93%; originating tissues, n = 7, 8.83%; total
778 cells, n = 8,857, 99.31%; UMAP1 SD, 2.77, 90.69%; UMAP2 SD, 2.49, 0.36%. **C**, UMAP of cells
779 in the central region colored by anchorage status. Turquoise, solid tumor; orange, CTCs. **D**,
780 Heatmap of RNA velocity correlations among AST factor, ECM, integrin, superoxide resistance
781 genes, and EMT genes.

782 **Table S1. Overview of patient information used for single cell transcriptome analysis.**

Patient #	Metastasis tissue	Subtype	Total cell counts			Cancer cell counts		
			Tumor	Blood	Meta	Tumor	Blood	Meta
patient1	liver	Her2	1,746	7,209	2,411	659	2	1,033
patient2	neck	Luminal-B	13,246	9,499	-	9,198	-	-
patient3	lung	Her2	14,254	25,180	11,982	516	1	2,531
patient4	lung	Luminal-B	-	25,394	10,900	-	2	7,507
patient5	brain	Her2	1,569	19,071	-	82	1	-
patient6	lung	TNBC	3,612	13,166	5,034	324	1	19
patient7	lymph	Luminal-A	9,572	26,768	9,404	4,438	8	5,833
patient8	neck	TNBC	11,741	9,117	12,746	1,257	7	13
patient9	liver	Luminal-A	8,077	21,471	16,458	5,032	9	11,641
patient10	lymph	TNBC	5,795	14,629	10,138	4,721	19	13
			69,612	171,504	79,073	26,227	50	28,590

783

784 **Movie S1. Dissemination assay of various breast cancer cell lines**

785 **A**, Video of MCF7 cell proliferation in the dissemination assay.

786 **B**, Video of BT549 cell proliferation in the dissemination assay.

787 **C**, Video of HS578T cell proliferation in the dissemination assay.

788 **D**, Video of MDA-MB-231 cell proliferation in the dissemination assay.

789

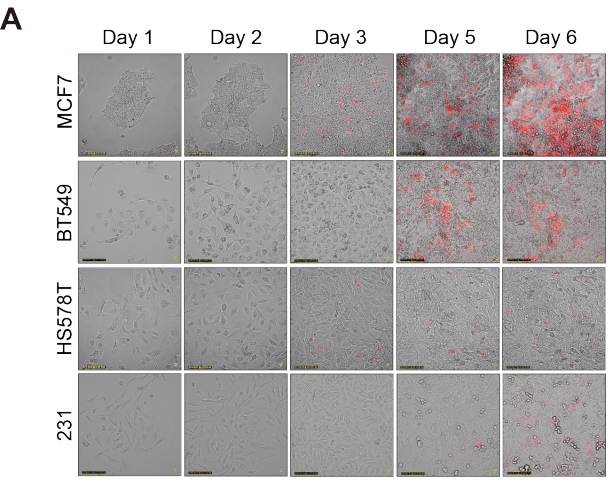
A
Day 1
Day 2
Day 3
Day 5
Day 6
MCF7
BT549
HS578T
231

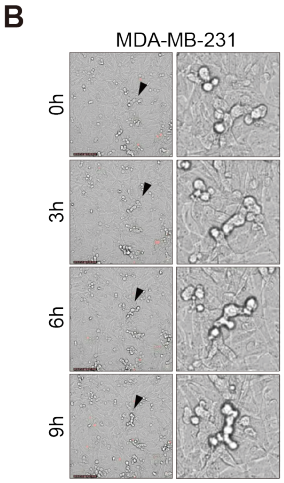
B
MDA-MB-231
0h
3h
6h
9h

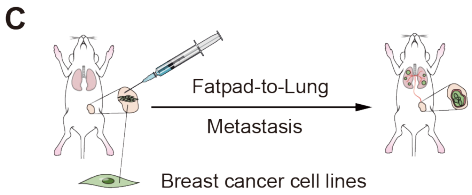
C
Fatpad-to-Lung
Metastasis
Breast cancer cell lines

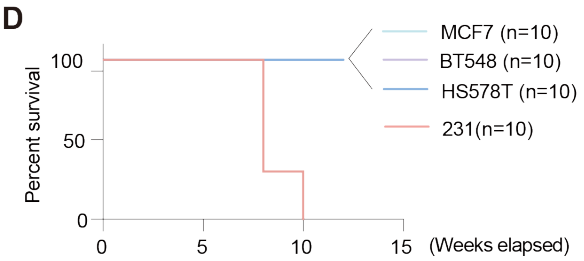
D
Percent survival
100
50
0
0
5
10
15
(Weeks elapsed)
MCF7 (n=10)
BT548 (n=10)
HS578T (n=10)
231(n=10)

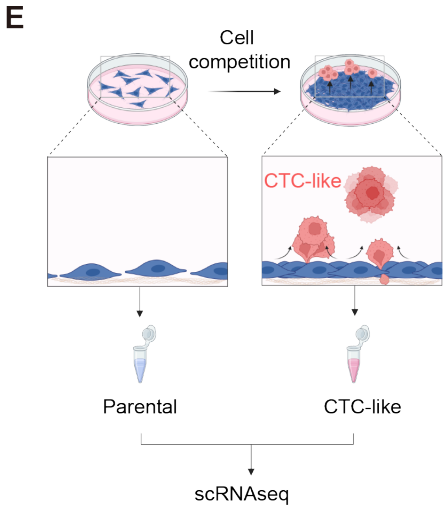
E
Cell
competition
CTC-like
Parental
CTC-like
scRNAseq

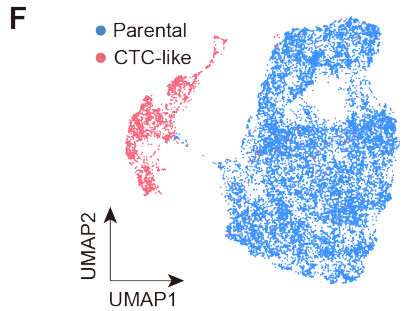
F
Parental
CTC-like
UMAP2
UMAP1

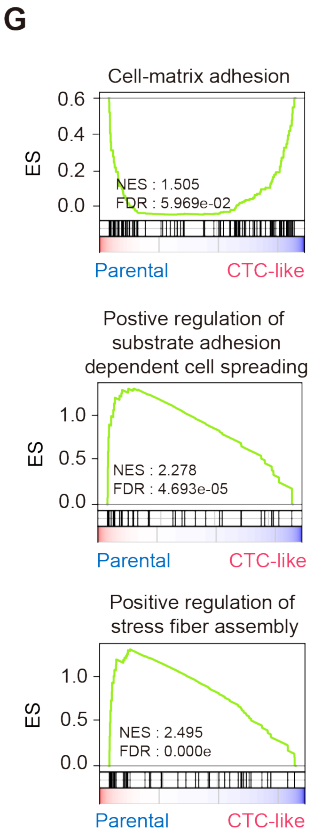
G
Cell-matrix adhesion
ES
NES : 1.505
FDR : 5.969e-02
Parental
CTC-like
Postive regulation of
substrate adhesion
dependent cell spreading
ES
NES : 2.278
FDR : 4.693e-05
Parental
CTC-like
Positive regulation of
stress fiber assembly
ES
NES : 2.495
FDR : 0.000e
Parental
CTC-like

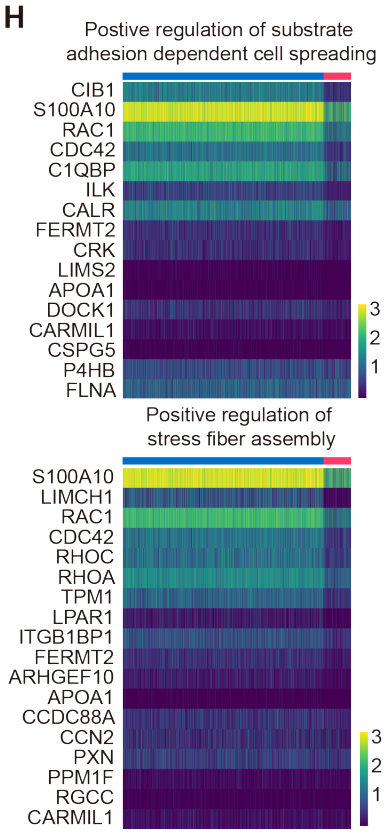
H
Postive regulation of substrate
adhesion dependent cell spreading
CIB1
S100A10
RAC1
CDC42
C1QBP
ILK
CALR
FERMT2
CRK
LIMS2
APOA1
DOCK1
CARMIL1
CSPG5
P4HB
FLNA
Positive regulation of
stress fiber assembly
S100A10
LIMCH1
RAC1
CDC42
RHOC
RHOA
TPM1
LPAR1
ITGB1BP1
FERMT2
ARHGEF10
APOA1
CCDC88A
CCN2
PXN
PPM1F
RGCC
CARMIL1

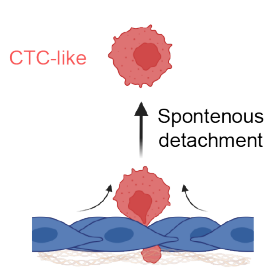
I
CTC-like
Spontenous
detachment

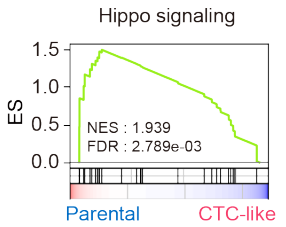
J
Hippo signaling
ES
NES : 1.939
FDR : 2.789e-03
Parental
CTC-like

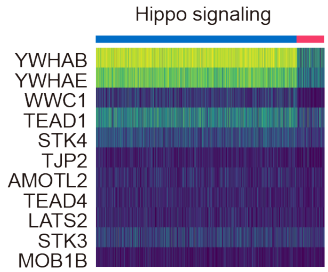
K
Hippo signaling
YWHAB
YWHAE
WWC1
TEAD1
STK4
TJP2
AMOTL2
TEAD4
LATS2
STK3
MOB1B

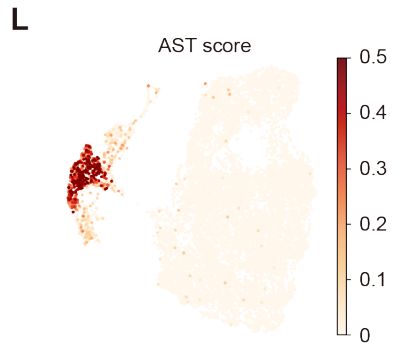
L
AST score

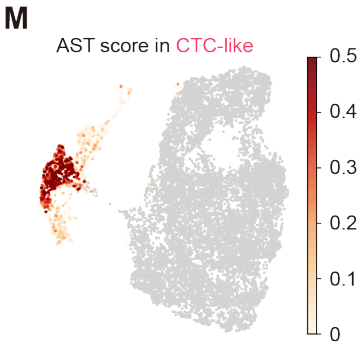
M
AST score in CTC-like

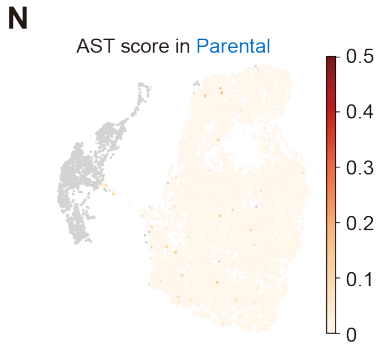
N
AST score in Parental

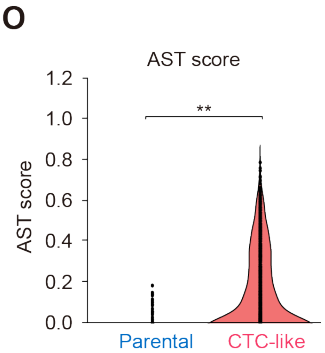
O
AST score
AST score
**
Parental
CTC-like

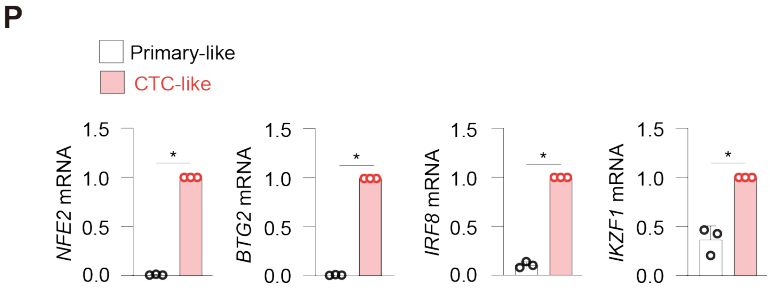
P
Primary-like
CTC-like
NFE2 mRNA
BTG2 mRNA
IRF8 mRNA
IKZF1 mRNA

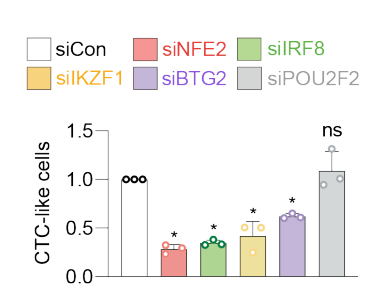
Q
siCon
siNFE2
siIRF8
siIKZF1
siBTG2
siPOU2F2
CTC-like cells
ns

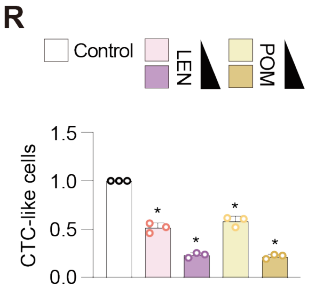
R
Control
LEN
POM
CTC-like cells

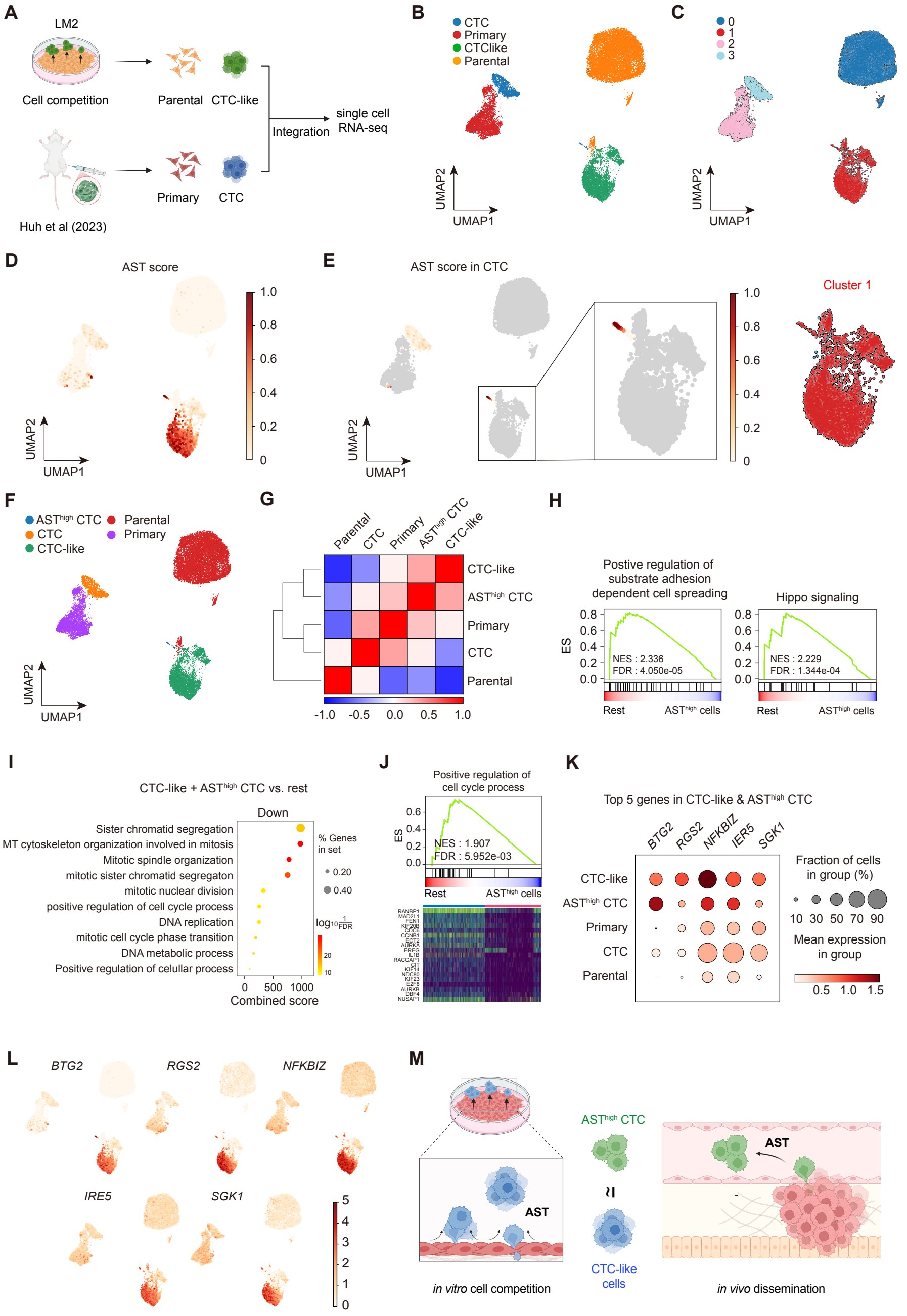
A
LM2
Cell competition
Parental
CTC-like
Integration
single cell RNA-seq
Primary
CTC
Huh et al (2023)
B
CTC
Primary
CTClike
Parental
UMAP2
UMAP1
C
0
1
2
3
UMAP2
UMAP1
D
AST score
1.0
0.8
0.6
0.4
0.2
0
UMAP2
UMAP1
E
AST score in CTC
Cluster 1
1.0
0.8
0.6
0.4
0.2
0
UMAP2
UMAP1
F
ASThigh CTC
CTC
CTC-like
Parental
Primary
UMAP2
UMAP1
G
Parental
CTC
Primary
ASThigh CTC
CTC-like
CTC-like
ASThigh CTC
Primary
CTC
Parental
-1.0
-0.5
0.0
0.5
1.0
H
Postive regulation of substrate adhesion dependent cell spreading
ES
NES : 2.336
FDR : 4.050e-05
Rest
ASThigh cells
Hippo signaling
NES : 2.229
FDR : 1.344e-04
Rest
ASThigh cells
I
CTC-like + ASThigh CTC vs. rest
Down
Sister chromatid segregation
MT cytoskeleton organization involved in mitosis
Mitotic spindle organization
mitotic sister chromatid segregaton
mitotic nuclear division
positive regulation of cell cycle process
DNA replication
mitotic cell cycle phase transition
DNA metabolic process
Positive regulation of celullar process
% Genes in set
0.20
0.40
log10 1/FDR
20
10
0
500
1000
Combined score
J
Positive regulation of cell cycle process
ES
NES : 1.907
FDR : 5.952e-03
Rest
ASThigh cells
RANBP1
MAD2L1
FEN1
KIF20B
CDC6
CCNB1
ECT2
AURKA
EREG
IL1B
RACGAP1
CIT
KIF14
NDC80
KIF23
E2F8
AURKB
DBF4
NUSAP1
K
Top 5 genes in CTC-like & ASThigh CTC
BTG2
RGS2
NFKBIZ
IER5
SGK1
CTC-like
ASThigh CTC
Primary
CTC
Parental
Fraction of cells in group (%)
10
30
50
70
90
Mean expression in group
0.5
1.0
1.5
L
BTG2
RGS2
NFKBIZ
IRE5
SGK1
5
4
3
2
1
0
M
AST
in vitro cell competition
ASThigh CTC
CTC-like cells
AST
in vivo dissemination

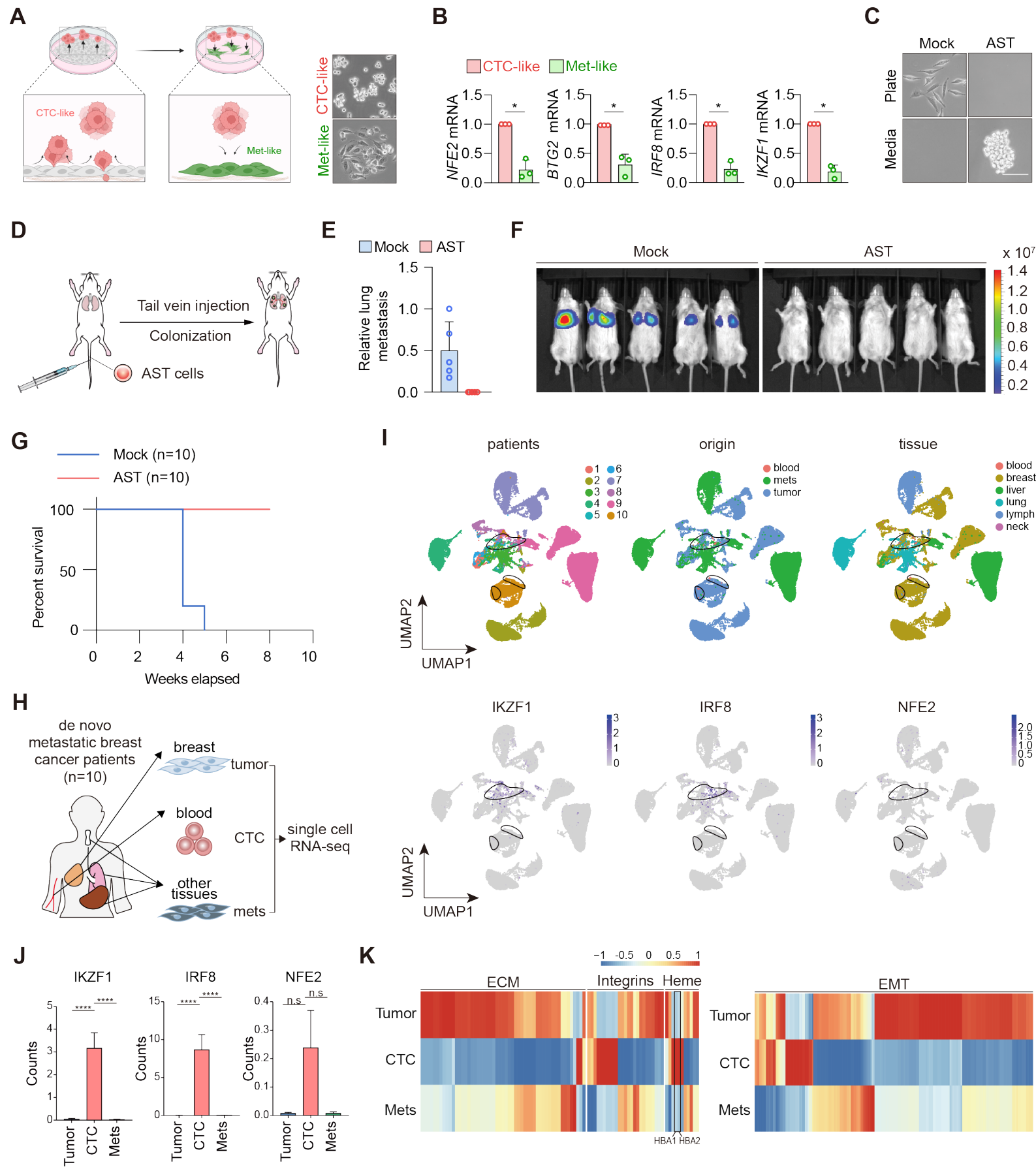
A
CTC-like
Met-like
CTC-like
Met-like
B
CTC-like
Met-like
NFE2 mRNA
BTG2 mRNA
IRF8 mRNA
IKZF1 mRNA
C
Mock
AST
Plate
Media
D
Tail vein injection
Colonization
AST cells
E
Mock
AST
Relative lung metastasis
F
Mock
AST
x 10^7
G
Mock (n=10)
AST (n=10)
Percent survival
Weeks elapsed
H
de novo metastatic breast cancer patients (n=10)
breast
tumor
blood
CTC
other tissues
mets
single cell RNA-seq
I
patients
origin
tissue
blood
mets
tumor
blood
breast
liver
lung
lymph
neck
UMAP2
UMAP1
IKZF1
IRF8
NFE2
J
IKZF1
IRF8
NFE2
Counts
Tumor
CTC
Mets
K
ECM
Integrins
Heme
EMT
Tumor
CTC
Mets
HBA1
HBA2

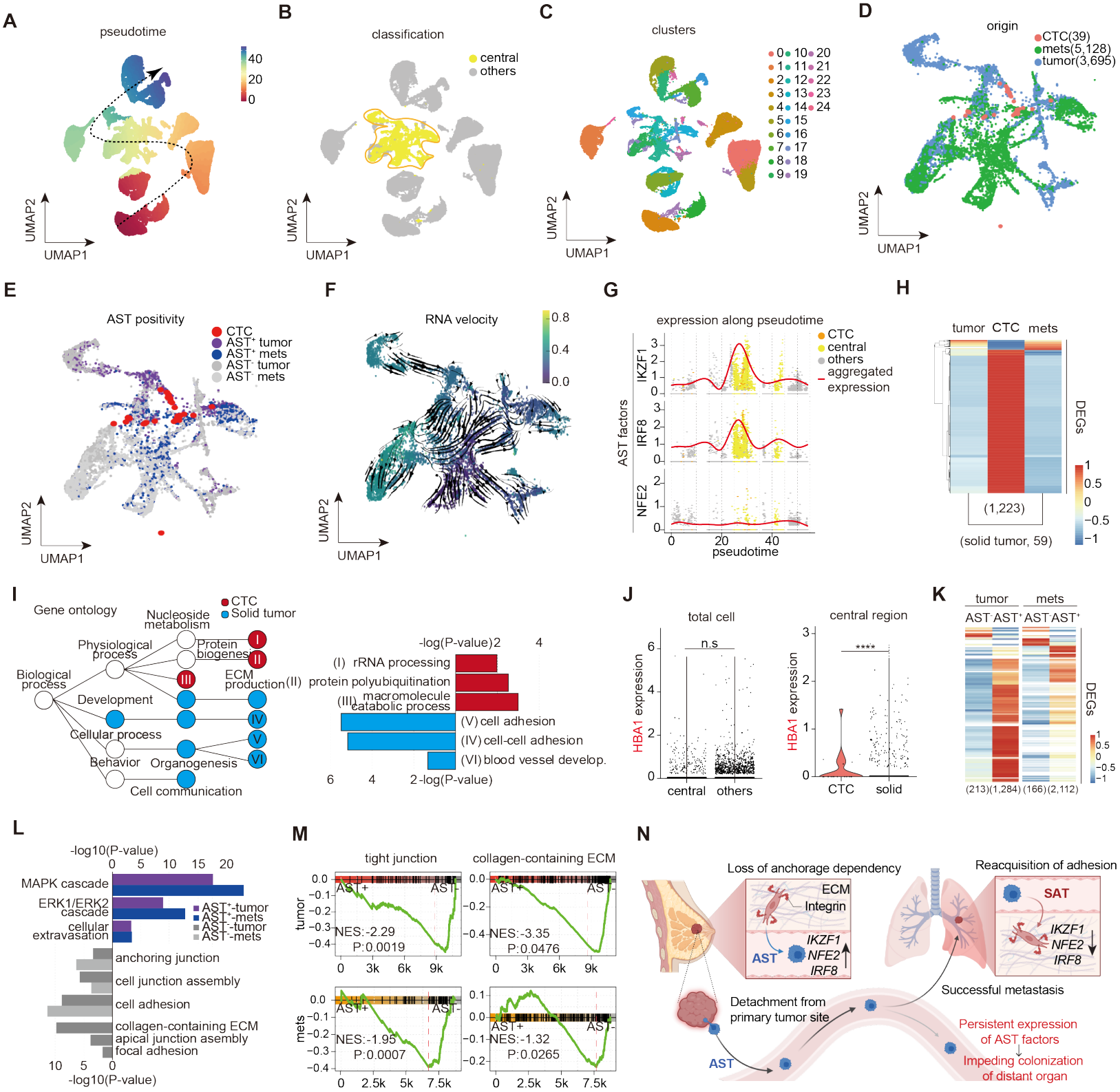
A
pseudotime
40
20
0
UMAP2
UMAP1
B
classification
central
others
C
clusters
0 10 20
1 11 21
2 12 22
3 13 23
4 14 24
5 15
6 16
7 17
8 18
9 19
D
origin
CTC(39)
mets(5,128)
tumor(3,695)
E
AST positivity
CTC
AST+ tumor
AST+ mets
AST- tumor
AST- mets
F
RNA velocity
0.8
0.4
0.0
G
expression along pseudotime
CTC
central
others
aggregated expression
AST factors
IKZF1
IRF8
NFE2
pseudotime
H
tumor CTC mets
DEGs
(1,223)
(solid tumor, 59)
I
Gene ontology
CTC
Solid tumor
Nucleoside metabolism
Physiological process
Protein biogenesis
Biological process
ECM production
Development
Cellular process
Behavior
Organogenesis
Cell communication
-log(P-value)
(I) rRNA processing
protein polyubiquitination
(III) macromolecule catabolic process
(V) cell adhesion
(IV) cell-cell adhesion
(VI) blood vessel develop.
-log(P-value)
J
total cell
central region
n.s
****
HBA1 expression
central
others
CTC
solid
K
tumor
mets
AST- AST+ AST- AST+
DEGs
(213)(1,284) (166)(2,112)
L
-log10(P-value)
MAPK cascade
ERK1/ERK2 cascade
cellular extravasation
AST+-tumor
AST+-mets
AST--tumor
AST--mets
anchoring junction
cell junction assembly
cell adhesion
collagen-containing ECM
apical junction asembly
focal adhesion
-log10(P-value)
M
tight junction
collagen-containing ECM
tumor
mets
AST+
AST-
NES:-2.29
P:0.0019
NES:-3.35
P:0.0476
NES:-1.95
P:0.0007
NES:-1.32
P:0.0265
N
Loss of anchorage dependency
ECM
Integrin
AST
IKZF1
NFE2
IRF8
Reacquisition of adhesion
SAT
Detachment from primary tumor site
Successful metastasis
Persistent expression of AST factors
Impeding colonization of distant organ